UCRL- 102239
PREPRINT

On the Refraction of Shock Waves at a Slow-Fast Gas Interface

L. F. Henderson
University of Sydney
Sydney, Australia

P. Colella
University of California
Berkeley, California

E. G. Puckett
Lawrence Livermore National Laboratory
Livermore, California

This paper was prepared for submittal to the
Journal of Fluid Mechanics

October 1989

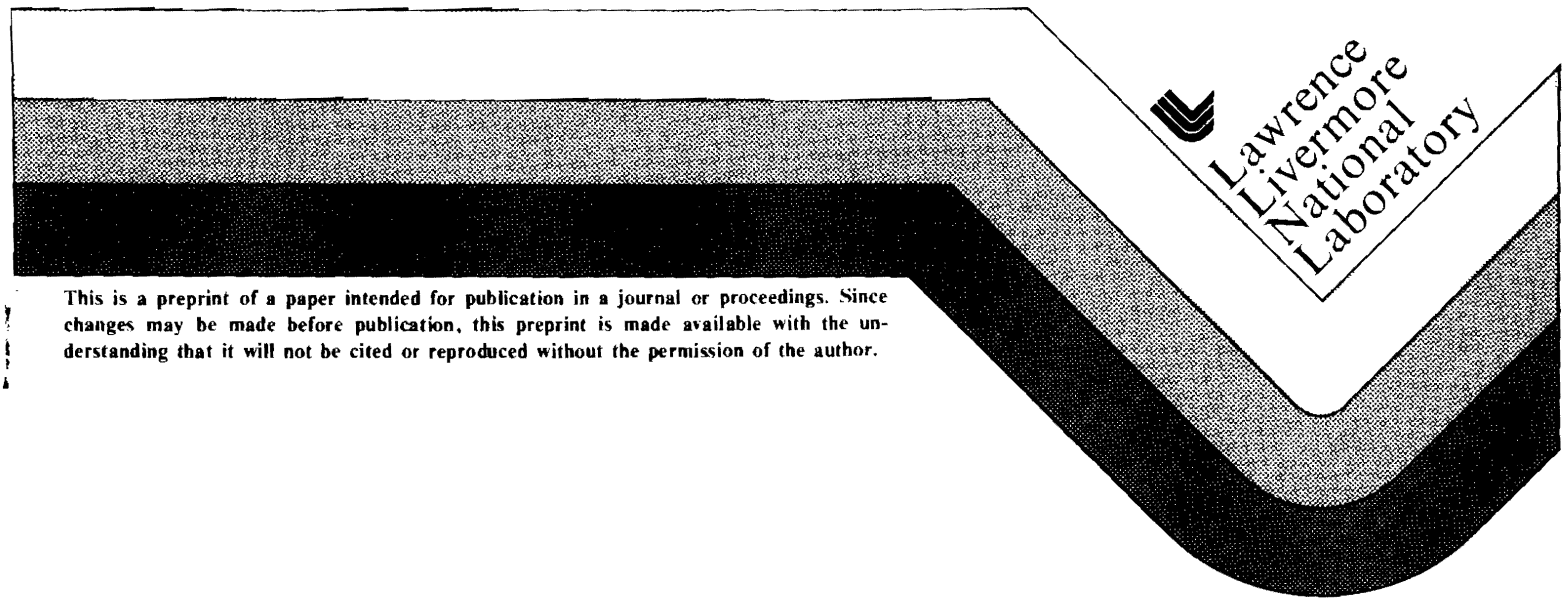

DISCLAIMER

On the Refraction of Shock Waves at a Slow-Fast Gas Interface*

L. F. Henderson†, P. Colella‡, and E. G. Puckett

L-316

Lawrence Livermore National Laboratory

Livermore, California 94550, USA

We present the results of our calculations on the refraction of a plane shock wave at a CO_2/CH_4 gas interface. The numerical method was an operator split version of a second order Godunov method, with automatic grid refinement. We solved the unsteady, two-dimensional, compressible, Euler equations numerically, assuming perfect gas equations of state. We compared our results with the experiments of Abd-El-Fattah and Henderson. Good agreement was obtained when the artifacts of the experiments were taken into account; especially the contamination of the CH_4 by the CO_2. A remaining discrepancy was ascribed to the uncertainty in measuring a wave angle due to the sharp curvature of the transmitted wave in the CH_4. All the main features of the regular and irregular refractions were resolved numerically for shock strengths that were weak, intermediate, or strong. These include free pre-cursor shock waves in the intermediate and strong cases, and evanescent (smeared out) compressions in the weak case, and the appearance of an extra expansion wave in the bound pre-cursor refraction.

1. Introduction

We consider two gases meeting along a plane interface, and we assume for simplicity that both them obey the perfect gas equation of state (Figure 1). We suppose that a plane incident shock i of wave velocity

* Work performed under the auspices of the U.S. Department of Energy at the Lawrence Livermore National Laboratory under contract number W-7405-ENG-48 and partially supported by the Applied Mathematical Sciences subprogram of the Office of Energy Research under contract number W-7405-Eng-48 and the defense Nuclear Agency under IACRO 88-873.

† Permanent address: Department of Mechanical Engineering, University of Sydney, Sydney NSW 2006, Australia

‡ Permanent address: Department of Mechanical Engineering, University of California, Berkeley, California 94720, USA.

U_i is propagated into one of the gases by the impulsive motion of a rigid boundary, such as a piston which drives into the gas at a velocity $U_{pi} < U_i$. We also assume that all the boundaries of the system are adiabatic. Subsequently i meets the interface between the gases at an angle of incidence α_i measured with respect to the interface (Figure 2). The shock i now begins to pass from the first, or incident gas I, into the second, or receiving gas II, where it becomes the transmitted shock t. When its new velocity U_t differs in either magnitude and/or direction from U_i, then by definition i has been refracted. Formally the relative refractive index n is defined by,

$$n \equiv |U_i|/|U_t| \quad . \tag{1.1}$$

We will say that the refraction is slow-fast when $n < 1$; fast-slow when $n > 1$; but that there is no refraction when $n = 1$.

If the velocities of the gas upstream and downstream of the incident shock and relative to it are u_0 and u_1 respectively, then the piston velocity is,

$$U_{pi} = u_1 - u_0 \quad . \tag{1.2}$$

Coordinates may be taken which are at rest with respect to the gas upstream of i, so that $u_0 = 0$, and the boundary condition then becomes simply,

$$u_1 = U_{pi} \quad . \tag{1.3}$$

In general a reflected wave is also produced at the gas interface by the refraction (Figures 1,2). When the incident wave i is a shock then so also will be the transmitted wave t, but the reflected wave may be either an expansion e or a shock r (Henderson 1989). It is assumed that there is always continuity in the pressure P and in the particle velocity u across the interface. Following refraction this gives,

$$P_2 = P_t \quad , \tag{1.4}$$

$$u_2 = u_t \quad . \tag{1.5}$$

The nature of the reflected wave may be determined with the help of (1.4) and (1.5) together with the definition of the wave impedance Z. This is the increase in the pressure which must be applied to the gas in order to induce a unit particle velocity in it, for example,

$$Z_i \equiv \frac{P_1 - P_0}{u_1 - u_0} = \frac{P_1 - P_0}{U_{pi}} \quad , \tag{1.6}$$

with similar definitions for the other waves. Equation (1.6) amounts to the momentum equation, and with the aid of the continuity equation it may also be written as,

$$Z_i = \pm \left[- \left(\frac{P_1 - P_0}{\nu_1 - \nu_0} \right) \right]^{\frac{1}{2}} \quad , \tag{1.7}$$

where ν is the specific volume. This demonstrates that Z_i is an average adiabatic bulk modulus. Alternatively we may obtain,

$$Z_i = \pm u_0 / \nu_0 = \pm \rho_0 u_0 = \mp \rho_0 U_i \quad , \tag{1.8}$$

$$Z_i = \pm u_1 / \nu_1 = \pm \rho_1 u_1 \quad , \tag{1.9}$$

where ρ is the density, and where we have used the fact that in shock wave coordinates,

$$u_0 = -U_i \quad . \tag{1.10}$$

The pressure reflection and transmission coefficients may now be defined as,

$$R \equiv \frac{P_2 - P_1}{P_1 - P_0} \quad ; \qquad T \equiv \frac{P_t - P_0}{P_1 - P_0} \quad , \tag{1.11}$$

and they are easily rewritten in terms of the wave impedance with the help of (1.4–1.6) together with the definitions of Z_r and Z_t,

$$R = \frac{Z_r}{Z_i} \cdot \frac{Z_t - Z_i}{Z_r - Z_t} \quad , \tag{1.12}$$

$$T = \frac{Z_t}{Z_i} \cdot \frac{Z_i - Z_r}{Z_t - Z_r} \quad . \tag{1.13}$$

Similar definitions may be given for the shock intensity I as the average power flux through unit area in the direction of propagation, and for the total power transmitted. The coefficients (1.11) to (1.13) show that when the impedance increases during refraction $|Z_t| > |Z_i|$, then a reflected shock r will be reflected from the interface, back into the incident gas, but that when it decreases $|Z_t| < |Z_i|$, then we obtain a reflected expansion. When the impedances are equal $|Z_t| = |Z_i|$, there is no reflected wave even though the two gases may differ in composition or in states. If this condition occurs at a non-zero angle of incidence then the particular angle is called the *angle of intromission* $\alpha_i = \alpha_{im}$, as in acoustic theory. The wave i is still refracted at this condition because in general $n \neq 1$ when $\alpha_i = \alpha_{im}$ (Figure 2b).

The wave systems illustrated in Figures 2a, b, and c, are called *regular refractions* by analogy with von Neumann's (1943) classification of regular and Mach *reflections*. His theory of regular reflection is easily extended to regular refraction and the results are in good agreement with experiment (Jahn 1956, Abd-El-Fattah *et al.* 1976, Abd-El-Fattah and Henderson 1978a,b).

If a regular wave system is to exist, then all of its waves must travel at the same velocity U along the interface, and this fact gives immediately the *fundamental law of refraction*, namely,

$$U = \frac{U_i}{\sin \alpha_i} = \frac{U_t}{\sin \alpha_t} = \frac{U_r}{\sin \alpha_r} = \frac{U_j}{\sin \alpha_j} \quad , \tag{1.14}$$

where U_j is the velocity of any wave in the reflected and centered expansion wave, and α_j is the corresponding wave angle. Evidently, $|U_j| = a_j$, which is the local speed of sound. Under certain conditions this law may be violated, for example with a continuous increase in the parameter α_i the regular wave system may break up with the t shock moving ahead of the incident and reflected waves to form some type of irregular refraction with pre-cursor waves (Figures 2d, e, and f). In this event,

$$\frac{U_t}{\sin \alpha_t} > \frac{U_i}{\sin \alpha_i} = \frac{U_r}{\sin \alpha_r} = \frac{U_j}{\sin \alpha_j} \quad . \tag{1.15}$$

The refraction law may be combined with the definitions of n and Z as follows.

$$n \equiv \frac{|U_i|}{|U_t|} = \frac{\sin \alpha_i}{\sin \alpha_t} = \frac{\nu_i Z_i}{\nu_t Z_t} \quad . \tag{1.16}$$

Clearly we have,

(*i*) for slow-fast refraction, $n < 1$, then $\alpha_i < \alpha_t$, and the refracted shock t is steeper than the incident shock with respect to the gas interface;

(*ii*) for fast-slow refraction, $n > 1$, $\alpha_i > \alpha_t$, and t is less steep than i;

(*iii*) for $n = 1$, $\alpha_t = \alpha_i$, and the wave is not (bent) refracted.

Using the refraction law we may also write,

$$\cos \alpha_t = (1 - \sin^2 \alpha_t)^{\frac{1}{2}} = (1 - n^{-2} \sin^2 \alpha_i)^{\frac{1}{2}} \quad . \tag{1.17}$$

Thus $\cos \alpha_t$ becomes pure imaginary when $n^{-2} \sin^2 \alpha_i - 1 < 0$, that is when α_i exceeds the *normal critical*

angle, $\alpha_i > \alpha_c$, which is defined for $\alpha_t = \pi/2$,

$$\sin \alpha_c = |U_i|/|U_t| \equiv n \quad . \tag{1.18}$$

Clearly α_c only exists for slow-fast refraction, $n < 1$. At the critical condition, t is perpendicular to the gas interface $\alpha_t = \pi/2$, that is, it is a normal shock. Accordingly the gas interface is not deflected in this special case and it remains everywhere in a single plane. It follows that when the pressure P_2 is applied to the receiving gas it causes no deflection of the interface, so that it behaves like a rigid surface. In this sense $|Z_t| = \infty$, when $\alpha_i = \alpha_c$. In summary, n is a measure of capacity of the gases to bend or refract the incident shock, while the wave impedances determine the nature of the reflected and transmitted waves. For oblique refraction it is convenient to generalize the definition of wave impedance to,

$$Z_i \equiv \frac{P_1 - P_0}{U_{pi} \cos \beta_i} \quad , \tag{1.19}$$

where β_i is the wave angle measured with respect to the *disturbed* gas interface (Figure 2). Similar expressions are defined for the other waves, and with these definitions (1.11) to (1.13) remain valid; (1.16) may also be used by introducing the factor $\cos \beta_i / \cos \beta_t$.

The von Neumann theory is inadequate for describing irregular refractions, because it can only describe the uniform regions of flow near a refraction point. But irregular systems have non-uniform flow regions and it is necessary to solve the equation of motion everywhere in order to obtain an adequate description of the phenomena. In the present paper, we present the results of our numerical studies of slow-fast refraction with particular emphasis on the irregular systems. The numerical method that we used is an adaption of a second order, finite difference solution of the Euler and continuity equations for the two-dimensional, unsteady, compressible flow of perfect gases. It is an operator split version of the second order Godunov method developed by van Leer (1979), Colella and Glaz (1985), and Colella and Woodward (1985). The results are compared with the experimental data of Abd-El-Fattah and Henderson (1978b). Agreement with

experiment is satisfactory for much of the data, if allowance is made for the effects of gas contamination in the experiments. Some discrepancies do exist, especially for the α_t data for irregular systems. This is ascribed to uncertainties in the measurements caused by the sharp curvature of the transmitted wave.

2. The Experiments

The experimental method has been described by Bitondo (1950), Jahn (1956), Abd-El-Fattah *et al.* (1976), and Abd-El-Fattah and Henderson (1978a,b). The experiments of the last named authors appear to be the most extensive and we describe them briefly. A delicate polymer membrane was set up in a shock tube; its functions were to define the gas interface as a plane surface, and to prevent the gases from mixing until the incident shock arrived. The mass of the membrane was between 0.5 and 1.0 $\times 10^{-4}$ kg m^{-2}, and its thickness was between 5.5 and 6.5 $\times$ 10^{-8} m. In order to set up a slow-fast interface such as CO_2/ CH_4, the CO_2 was slowly introduced onto one side of the membrane while the CH_4 was introduced onto the other. The gases were continuously circulated through the shock tube to minimize mutual contamination by diffusion and leakage across the membrane. The contamination was monitored continuously by a thermal conductivity meter, and typically the CH_4 was contaminated by about 10% by volume with CO_2, but the CO_2 was much purer. It should be noted that the volume of CO_2 in the shock tube was about 250 times larger than the CH_4.

A shock of prescribed inverse strength $\xi_i \equiv P_0/P_1$, was started in the CO_2, and arranged to strike the membrane/gas interface at a pre-determined angle of incidence α_i. The shock shattered the membrane and entered the CH_4, and was thus refracted. The wave system was photographed by a schlieren optical system, and transducers measured the speed and strength of the incident shock.

Recently, Haas and Sturtevant (1987) have experimented with weak shocks refracting at cylindrical and spherical interfaces. The gases were initially prevented from mixing by the use of plastic membranes or soap bubbles. However, in the interest of simplicity we will confine our attention to plane gas interfaces.

3. The Computations

3.1. The numerical method

We used a second order finite difference solution of the Euler and continuity equations on a rectangular grid with reflecting boundary conditions on three sides and inflow boundary conditions on the fourth. The numerical integration of the equations was accomplished by using an operator split version of a second order Godunov procedure (van Leer 1979, Colella and Woodward 1984). In our implementation we employed an efficient algorithm for the solution of the Riemann problem (Colella and Glaz 1985). Since the method is a conservative finite difference scheme, mass, momentum, and energy were all conserved. The method is accurate to second order in space and time for smooth flow, and captures shocks and other discontinuities with minimum numerical overshoot and dissipation. It has been used quite extensively to compute unsteady shock reflections in gases, with a demonstrated ability to resolve complex interactions of discontinuities with good agreement with experiment (Glaz *et al.* 1985).

An important feature of the numerical method is that it employs a dynamic regridding strategy called adaptive mesh refinement (AMR) in order to refine the solution in regions of particular interest or excessive error. This is accomplished by placing a finer, rectangular grid over any such region, with the grid spacing being reduced by an even factor which is typically either 2 or 4. The boundary of the refined grid always coincided with the cell edges of the coarse grid. Multiple levels of refinement were possible with the maximum number of nested grids being supplied as a parameter by the user. In the present work, we determined those regions which required refinement by estimating the local truncation error in the density, and refining wherever the error was greater than an initially specified amount. Special care was taken to ensure the correct fluxes on boundaries between coarse and fine grids; the details are given by Berger and Colella (1987). Adaptive gridding was a crucial component of our method which enabled us to resolve important features of the flow economically. A typical run with two levels of gridding and with a refinement factor of 2 took about 5 to 10 minutes of CPU time on a CRAY XMP computer.

The gas interface was modelled using an algorithm of Noh and Woodward (1976). Here a number, f_{ij}

between 0 and 1, and called the volume fraction was associated with each grid cell through which the gas interface passed. This f_{ij} was the volume fraction of the cell occupied by one of the gases. Obviously the other gas occupied the fraction $1 - f_{ij}$. At the end of every time step a simple picture of the interface consisting entirely of vertical and horizontal line segments was constructed from the volume fraction information. This was used to determine how much of each gas was convected out of the cell and into adjacent cells at this timestep, and hence to update the volume fractions associated with each cell. One of the drawbacks of the SLIC algorithm is that in a region undergoing expansion or compression both of the gases in a multi-gas cell will be expanded or compressed equally, in spite of the density differences that may exist between them. To use this method with the present problem we incorporated a scheme due to Colella *et al.* (1989) in which the equations of gas dynamics are supplemented with evolution equations for the volume fraction, total energy, and mass density of each gas in the multi-gas cells. This formulation takes into account the compressibilty of each gas component in a multifluid cell so as to ensure the correct individual expansions or compressions.

3.2. Outline and plan of the numerical work

We shall present the results of our computations as though we had done a series of experiments in a shock tube. This means that in a particular sequence, the ratios of the specific heats γ_i, γ_t, of the gases and their molecular weights μ_i, μ_t were held constant and so also was ξ_i. The only parameter that varied through the sequence was α_i. This was assumed to be initially near the condition for head-on incidence at $\alpha_i = 0$; it was then increased in discrete steps until it approached glancing incidence at $\alpha_i = \pi/2$; thus $0 < \alpha_i < \pi/2$. A particular refraction was uniquely defined once the values of $(\gamma_i, \gamma_t, \mu_i, \mu_t, \xi_i, \alpha_i)$ together with the system boundaries were given. Typically the phenomena that appeared from this procedure were a sequence of regular refractions followed by an irregular sequence.

We shall compare our numerical results with the experimental data obtained by Abd-El-Fattah and Henderson (1978b) for the slow-fast, $n < 1$, CO_2/CH_4 gas interface. There were two artifacts in those experiments which we took into account in our calculations in order to make the comparison as accurate as possible. These were the inertia of the membrane and the contamination of the gases by diffusion and

leakage across it.

Membrane Inertia: We calculated the membrane density from the published data, and it was about 680 time denser than CO_2 at standard conditions. Using this factor in the calculations, the membrane was treated as though it were super dense carbon dioxide. Generally its effect was negligible; all we noticed was a slight displacement in the pressure contours when the contours were compared with, and without, the membrane for the same refractions. In view of this we deleted it from the remainder of our calculations.

Gas Contamination: The published data showed that the methane was contaminated by about 10% by volume with carbon dioxide, but that the CO_2 itself was approximately pure. (Remember their volume ratio in the shock tube was about 250:1 in favor of the CO_2.) The properties for the pure and contaminated gases are presented in Table 1. Contamination is a significant effect and it will be discussed below.

	Pure carbon dioxide	**Pure methane**	**Contaminated methane**
γ	1.288	1.303	1.301
μ_i	44.01	16.04	18.84

Table 1. Properties of the pure and contaminated gases.

4. Results and Discussion for a Weak Shock Refraction Sequence

4.1. The polar diagrams

The sequence and its polar diagrams are presented in Figure 3, they are similar to the ones described by Abd-El-Fattah and Henderson. When α_i is comparatively small, there is a regular refraction with a reflected expansion (RRE), (Figure 3a), so $|Z_t| < |Z_i|$, $R < 0$, $T > 0$. Since the refraction is slow-fast $n < 1$, we have by (1.16) that $\alpha_t > \alpha_i$, that is, t is steeper than i. The reflection e, is a centered, Prandtl-Meyer, expansion fan and it is plotted in the polar diagram as the isentropic curve c. It intersects the polar for the t shock at

the point ϵ_1 which defines the von Neumann solution for RRE. The solution requires there to be continuity in the pressure and in the streamline direction δ, everywhere along the gas interface. Although (1.4) remains valid when $\alpha_i \neq 0$, (1.5) must be replaced by,

$$\delta_0 + \delta_1 = \delta_t \quad , \tag{4.1}$$

which is the continuity condition for the streamline direction. It is sometimes necessary to replace (1.4) and (4.1) by the equivalents,

$$(P_2 - P_1) + (P_1 - P_0) = (P_t - P_0) \quad , \tag{4.2}$$

$$U_{pi} \cos \beta_i + \int_1^2 \cos \beta_j \, dU_{pj} = U_{pt} \cos \beta_t \quad , \tag{4.3}$$

where U_{pi}, U_{pt}, are the driving piston velocities of the i and t shocks, dU_{pj} is the infinitesimal withdrawing piston velocity for an arbitrary jth wave in the reflected expansion, and β_i, β_t, β_j, are the wave angles which are defined with respect to the *disturbed* gas interface (Figure 2).

If α_i is now increased continuously, the polars shrink somewhat and the intersection point A_1 moves downwards towards the point i which is the map of the incident shock. As this happens the strength $|P_2 - P_1|$ of the expansion decreases and eventually vanishes at the angle of intromission $\alpha_i = \alpha_{im} \approx 32.0592°$, which corresponds to $\epsilon_1 \equiv i \equiv A_1$ where A_1 is the intersection point of the primary polars (i,t). The reflection is reduced to a Mach line degeneracy $|P_2 - P_1| = 0$ and the other wave impedances become equal $Z_t = Z_i$, $R = 0$, $T = 1$, this is the condition for *total transmission*, and here also $\alpha_t > \alpha_i$ (Figure 3b). As α_i continues to increase $\alpha_i > \alpha_{im}$, the reflection becomes a shock, (RRR) (Figure 3c), and now $|Z_t| > |Z_i|$, $R > 0$, $T > 0$, with again $\alpha_t > \alpha_i$. The von Neumann theory gives two solutions λ_1 and λ_2 for RRR, but experiment shows that it is the weaker λ_1 solution which appears physically. In this respect note that λ_1 is the continuation of the ϵ_1 solution while λ_2 is not; in fact at the intromission angle, ϵ_1 and λ_1 are identical and degenerate, $\epsilon_1 \equiv \lambda_1 \equiv A_1 \equiv i$.

As α_i continues to increase, λ_1 and λ_2 approach each other and eventually coincide, $\lambda_1 \equiv \lambda_2$ (Figure 3d). This takes place at the *shock critical angle* $\alpha_i = \alpha_{sc} = 34.488°$. In general this angle does *not* coincide with the *normal critical angle* α_c, defined by (1.18), and usually occurs before it, $\alpha_{sc} < \alpha_c$. For $\alpha_i > \alpha_{sc}$, the λ_1 and λ_2 solutions are no longer physically significant because they are unreal. The refraction is now irregular and pre-cursor compression waves may develop (Figures 3e-g). In the experiments of both Jahn and Abd-El-Fattah and Henderson the pre-cursors did not appear as soon as the shock critical angle was exceeded. In fact α_i had to increase somewhat beyond α_{sc} before they were observed. We will return to this point later.

4.2. The numerical results for the sequence

The numerical results presented here are all for uncontaminated gases with no membrane. We believe that these results will be of more general interest than those which include the artifacts of the experiments. Selected contour plots for the sequence are shown in Figure 4, a schlieren photograph from the experiments is shown in Figure 5a and color graphics to compare with the schlieren photograph are shown in Figures 5b,c,d (Plates 1, 2). Of course the comparison can only be qualitative because the numerical results do not include the artifacts.

4.3. Structure of the weak irregular refraction systems

4.3.1. The bound pre-cursor refraction system, BPR

The regular systems RRE and RRR are well described by the von Neumann theory, and in more detail by our numerical results. When the shock critical angle is exceeded $\alpha_i > \alpha_{sc} \approx 34.4885°$, the RRR system becomes augmented with an expansion wave which appears in the receiving gas (CH_4), and with its pressure contours apparently centered on the refraction point R (Figures 3e, 4e). The contours at first diverge as they move away from R, but then swing around and refract into the incident gas (CO_2) where they converge into a compression downstream of the reflected shock r. According to the von Neumann theory, there are no physically acceptable solutions for $\alpha_i > \alpha_{sc}$, and the impedance of the gases are unreal. For those reasons

the system is irregular. The r and t shocks now have sharply increased curvatures near R, and furthermore t is now everywhere inclined forward of R, $\alpha_t > \pi/2$ (Figures 4e,f). By contrast for the regular systems, t is everywhere inclined backwards, $\alpha_t < \pi/2$ (Figures 4a-d). Thus t is a pre-cursor wave for $\alpha_i > \alpha_{sc}$ and in the special case shown in Figures 3c and 4e, the t wave moves along the gas interface at the same velocity as i and r, that is Equation (1.14) remains satisfied, it is also a *bound* pre-cursor. With Abd-El-Fattah and Henderson we will call this irregular system a "bound precursor refraction" (BPR).

4.3.2. The conditions for the RRR $\rightleftharpoons$ BPR transition

The shock critical angle α_{sc} is defined by the double root $\lambda_1 \equiv \lambda_2$, of the von Neumann theory (Figure 3d), and this amounts to a generalization of the well known shock detachment criterion for regular/irregular transition in shock *reflection*. If we suppose that $|Z_t|$ increases without limit, $|Z_t| \rightarrow \infty$, then reflection can be thought of as a limiting case of refraction. Inspection of the polar diagram makes it clear that the rival (sonic) criterion for transition (Hornung and Taylor, 1982) does not exist for this refraction because the flow downstream of the reflected shock is supersonic $M_2 > 1$, all the way to the $\lambda_1 \equiv \lambda_2$ point. Thus, this point which corresponds to $\alpha_i = \alpha_{sc}$ seems to be the only possibility for a transition criterion in weak refraction, RRR $\rightleftharpoons$ BPR.

The computational data indicates that transition occurs at $\alpha_i = \alpha_{sc}$, or very close to it, but experiment suggests that it is somewhat delayed beyond this point. However, the transition point is a little obscured in the experiments by the wire frame on which the membrane is mounted, and also by the presence of a thin film of silicone oil that was used to seal the wire to the shock tube windows in order to reduce gas leakage. In view of this, we conclude from the evidence available to us that transition either occurs at $\alpha_i = \alpha_{sc}$, or else very close to it.

It is interesting to note that the condition $\alpha_t = \pi/2$ must also be attained during the transition RRR $\rightarrow$ BPR, because as this occurs we have seen that $(\alpha_t < \pi/2) \rightarrow (\alpha_t > \pi/2)$. Therefore the condition corresponding to the normal critical angle α_c defined by Equation (1.18) is *forced* to occur at the same condition as the shock critical angle α_{sc}, even though $\alpha_{sc} < \alpha_c$.

4.3.3. The free pre-cursor refraction system, FPR

With steadily increasing α_i, the t wave eventually breaks loose from the i and r shocks and runs ahead of them along the gas interface (Figures 4f and g). The refraction law has now been violated as with expression (1.15), and there is now a *free* pre-cursor refraction (FPR) in which the t wave moves ever further ahead of i and r with time.

It will be noticed that the pressure contours for the t wave are now spread out at, and near, the gas interface (Figures 4f and g), instead of being concentrated as for a shock (Figure 4e). Thus t is a locally smeared out or *evanescent* wave. However, further away from the interface the contours do converge to form a coherent shock. The t wave is itself refracted from the CH_4 back into the CO_2, which means that its refraction is locally *fast-slow*, $n > 1$. The wave transmitted into the CO_2 is the side wave s, and it is also an evanescent wave (Figure 3f). Since locally, $n > 1$, then $|\alpha_t| > |\alpha_s|$. There appears to be no sign of a reflected wave from the $t - s$ refraction, nor does there seem to be one in the experiments, (presumably it is too weak to be resolved). Thus the local system appears to consist only of the $t - s$ pair. The s wave and the incident shock i eventually encounter, and mutually modify, each other. The s contours converge to the reflected shock r after passing through i. The modified shock k, continues to the disturbed gas interface where it is locally refracted with total internal reflection $R = -1$, $T = 0$, $Z_t = 0.$; this means that k is reflected as a centered expansion wave, e. This last wave eventually overtakes r and causes almost complete mutual cancellation, so that finally a weak reflection is propagated into the downstream CO_2.

It is natural to consider the conditions where a bound pre-cursor system becomes a free pre-cursor system or vice versa, BPR $\rightleftharpoons$ FPR. This is associated with the spreading out of the t wave into a distributed compression near the interface and it then runs ahead of the i and r shocks along the interface. Therefore the transition occurs with the violation of the refraction law, Equation (1.14), in other words (1.15) now applies. The law is of course immediately re-established for the pre-cursors,

$$\frac{U_s}{\sin \alpha_s} = \frac{U_t}{\sin \alpha_t} \quad . \tag{4.4}$$

4.3.4. The free pre-cursor von Neumann refraction system, FNR

Transition to yet another irregular refraction takes place as α_i continues to increase. It is characterized by a weak Mach reflection appearing in the CO_2. Some pressure contours of it are presented in Figure 4h and a schlieren photograph and color graphics in Figures 5a and b (Plates 3 and 4). Abd-El-Fattah and Henderson (1978) called it a "free pre-cursor von Neumann refraction" (FNR) see Figure 2f of this paper.

The conditions for the FPR $\rightleftharpoons$ FNR transition are not known and our calculations are not sufficiently detailed to form a hypothesis with any confidence, although we might conjecture that transition is associated with sonic flow downstream of t along the gas interface.

In summary the sequence of phenomena for the refraction of a weak shock at a slow-fast gas interface with increasing angle of incidence α_i is as follows.

$$\text{RRE} \rightleftharpoons \text{RRR} \rightleftharpoons \text{BPR} \rightleftharpoons \text{FPR} \rightleftharpoons \text{FNR} \quad .$$

This sequence seems to be generally well supported by both the computations and by the experiments.

4.4. Comparison of the numerical results with experiment

In the interests of making the comparison as precise as possible we used the same values of the parameters $(\gamma_i, \gamma_t, \mu_i, \mu_t, \xi_i, \alpha_i)$ for our input data as Abd-El-Fattah and Henderson measured in their experiments. This included using the data for the contaminated gas shown in Table 1, and the same boundary configuration. Some of the calculations were repeated for the pure gases in order to obtain an estimate of the sensitivity of the results to gas contamination. The numerical data for the pure and the contaminated gases are compared with experiment in Figures 6 and 7. Figure 6 shows a variety of wave angles as well as the trajectory path angle χ for the four waves $i - s - k - r'$. For the regular part of the sequence, RRE $\dashrightarrow$ RRR, the numerical results for the contaminated gas are everywhere in satisfactory agreement with experiment, but the corresponding results for the pure gases show a significant discrepancy for the α_t data, but not for the

α_r, α_e, data. So only the α_t data seems to be sensitive to contamination, and that sensitivity is greatest near transition $\alpha_i = \alpha_{sc}$, $\lambda_1 \equiv \lambda_2$, where small variations in the contamination can cause significant changes to α_t. Thus, the α_t data is sensitive to contamination while the other angle data are not. This is ascribed to the fact that incident and reflected waves propagate in the CO_2 which is little affected by contamination because of the large fraction of the volume it occupies in the shock tube, while the t wave propagates in the CH_4 and this *is* significantly affected (Table 1).

After transition to irregular refraction the numerical data for the contaminated gas is again in agreement with experiment so long as, approximately, $\alpha_i < 60°$; but a significant discrepancy is evident for $\alpha_i > 60°$. By contrast the data for the pure gases everywhere shows a larger discrepancy. For irregular refraction the t wave is everywhere curved, and for $\alpha_i > 60°$ we found that this curvature became quite sharp near the gas interface. This made it increasingly uncertain about where to draw the tangent to t in order to measure α_t at the interface. The same difficulty occurred for both the schlieren photographs and for the contour plots. We therefore looked for more robust data to compare with the experiment, and we found this in the measurements of the wave velocities U_i and U_t. The numerical data for $|U_t|/|U_i|$ is compared with experiment in Figure 7. These data include the calculations for the pure and the contaminated gases, and it will be noted that the results bracket the experiment data.

It should be remarked that the measurements of the gas contamination are only average values obtained after the contaminated gases had been drawn from the shock tube and individually sent to the thermal conductivity meter. Therefore the local contamination near the gas interface could have been significantly different from the average value obtained at the meter. In view of the uncertainties involved we conclude that the agreement between the numerical data and experiment is satisfactory.

5. Results and Discussion for a Strong Refraction Sequence

5.1. Wave structures in the sequence

A second series of computations was done for the CO_2/CH_4 interface, except that i was now a strong

shock $\xi_i = 0.18$; this work was restricted to the pure gases. Selected contours are presented in Figure 9, and a schlieren photograph together with color graphics are presented in Figure 10 (Plates 3,4). A comparison with experiment cannot be precise because the effect of gas contamination has not been taken into account in the calculations.

The polar diagrams are presented in Figure 11. When α_i is small enough to result in regular refraction, the von Neumann theory provides three physically acceptable solutions, namely two with reflected shocks λ_1, λ_2 and one with a reflected expansion ϵ_1 (Figure 11a). It was the ϵ_1 (RRE) solution which Abd-El-Fattah and Henderson observed. With increasing α_i one obtains the coincidence $\lambda_1 \equiv \lambda_2 \equiv i \equiv A_1$, and then the reflected shocks in the λ_1, λ_2, (RRR) solutions degenerate to Mach lines (Figure 11b). Although this takes place at the angle of intromission $\alpha_{ie} = 35.95°$, it has no physical significance in this case because ϵ_1 is not degenerate at this condition. Hence the impedances are *not* equal, $|Z_t| \neq |Z_i|$, for the solution ϵ_1 which is actually observed.

For $\alpha_i > \alpha_{ie}$, the λ_1, λ_2, solutions are unreal and at the same time we obtain a second solution ϵ_2 of the RRE type (Figure 11c). However, once more it was the ϵ_1 solution that Abd-El-Fattah and Henderson observed. Clearly, at $\alpha_i = \alpha_{ie}$ the coincidence can be extended to ϵ_2, thus, $\lambda_1 \equiv \lambda_2 \equiv \epsilon_2 \equiv i \equiv A_1$. Notice, however, that the ϵ_1 solution nowhere forms a coincidence with either of the λ_1, λ_2, solutions as it did at the A_1 point in the weak sequence. Consequently no refraction of the RRR type can appear in this strong sequence.

As α_i continues to increase one eventually obtains $\epsilon_1 \equiv \epsilon_2$ (Figure 11d), where the isentropic c is tangent to the t polar. This again occurs at the shock critical angle $\alpha_{sc} = 37.79°$, but it differs from the weak series in that the coincidence is an RRE type $\epsilon_1 \equiv \epsilon_2$, instead of the RRR type, $\lambda_1 \equiv \lambda_2$.

For $\alpha_i > \alpha_{sc}$, the refraction is irregular and both the experiments and the calculations agree that it is again a free pre-cursor system. However, the numerical results show that both the t and the s waves are shocks and not evanescent compressions as they were in the weak sequence. Structurally the system consists of the pre-cursor, transmitted-side shock pair $t - s$, interacting with a single Mach reflection triplet of shocks

$i - r_1 - n$ (Figure 11e). The side shock s, now interacts with the *Mach* shock n, modifies it and produces the second reflected shock r_2. Consequently, there are two Mach reflections in the incident gas, $i - n - r_1$, and $s - n - r_2$, the refraction will be called a "*twin Mach reflection-refraction*" (TMR). The r_2 shock undergoes total internal reflection at the disturbed gas interface and gives rise to the reflected expansion e, which in turn overtakes and attenuates r_1. Contact discontinuities cd_1 and cd_2 appear at the MR triple points (Figures 9e, 10a (Plate 3), and 11e); but they are not visible in Figure 10 (Plates 3 and 4). There are now three shear layers in the downstream flow, namely cd_1, cd_2, and the disturbed gas interface.

5.2. Comparison of the numerical results with experiment

The numerical results are compared with the experimental data in Figures 8 and 12. As expected the discrepancy for the α_t data is comparatively large because we did not take into account the gas contamination. Qualitatively it is similar to the discrepancy for the weak series in Figure 6. The increasing size of the discrepancy for the irregular refraction is again attributed to the uncertainty of measuring α_t with increasing curvature of the t shock near the interface. The other angle data, χ_1, χ_2, α_e, α_j, and δ_t, are generally in satisfactory agreement, granted the numerical and experimental uncertainties. These last measurements were made either for the CO_2 flow field, or along its boundary (δ_t), and, as we have seen, such measurements are insensitive to gas contamination. The curvature of the reflected shock r prevented us from making reliable measurements of α_r from our numerical plots.

The numerical data for $|U_t|/|U_i|$ display a small systematic discrepancy from the experimental data (Figure 12). This is qualitatively similar to the pure gas results shown in Figure 7, and is ascribed to the same cause, namely gas contamination. Nevertheless, the agreement with experiment is quite reasonable.

6. The Boundary Between the Strong and the Weak Systems

We consider how a weak irregular refraction may be changed into a strong one, or vice versa, FPR $\rightleftarrows$ TMR. This will be done by continuously reducing ξ_i from $\xi_i = 0.78$ where the system is weak, to $\xi_i = 0.18$,

where it is strong. For simplicity the other parameters (γ_i, γ_t, μ_i, μ_t, α_i) will be held constant as ξ_i varies. During this process one finds that the shock triple points F_1, F_2 (Figures 2d,3g) continuously approach the quadruple point G (Figure 2e) and then for some ξ_i they coincide with it, $F_1 \equiv F_2 \equiv G$. The weak Mach reflection has now vanished and the number of shocks in the incident gas are reduced to four, $i - s - r_1 - r_2$. If we imagine that the CH_4 is replaced by a rigid medium with the same boundaries, then the four-shock interaction would amount to the twin regular reflection studied by Smith (1959). Since the i and s shocks are generally of unequal strength, their interaction is asymmetrical and a contact discontinuity arises in the downstream flow. A schlieren photograph of this refraction, obtained by Abd-El-Fattah and Henderson with $\xi_i = 0.53$ is presented in Figure 13 (Plate 5), together with some color graphics from the calculations (Figure 13, Plates 5, 6). We will call it a twin regular reflection-refraction (TRR). Actually the cited authors found that this system existed for a range of ξ_i and not just for a particular value on the boundary between the strong and the weak systems. Eventually, however, as ξ_i becomes small enough the four shock system in the TRR transits into the twin Mach reflection characteristic of a TMR (Figure 10, plates 3, 4, and Figure 11). The condition for the TRR $\rightleftarrows$ TMR, transition have been discussed by Smith for reflection, and Abd-El-Fattah and Henderson for refraction.

A variety of special conditions may be used to define precisely the strong/weak boundary. Some of them have been discussed by the above authors. Here we notice that for weak systems the regular/irregular transition RRR $\rightleftarrows$ FPR takes place at the von Neumann tangency point. $\lambda_1 \equiv \lambda_2$, that is at α_{sc}, but for strong systems the tangency condition has a different character $\epsilon_1 \equiv \epsilon_2$, so RRE $\rightleftarrows$ TMR, but again at α_{sc}. It seems plausible therefore to define the strong/weak boundary at the point where *both* conditions are in coincidence, $\lambda_1 \equiv \lambda_2 \equiv \epsilon_1 \equiv \epsilon_2 \equiv i \equiv A_1$. For the pure gas interface CO_2/CH_4 this is approximately at $\xi_i = \xi_b = 0.471$, or $\alpha_i \equiv \alpha_b = 34.05°$. So an incident shock i has a weak refraction whenever $\xi_i > \xi_b$ and a strong one when $\xi_i < \xi_b$.

Abd-El-Fattah and Henderson used a different condition for the boundary. Theirs was based upon a generalization of the von Neumann classification for shock reflection, but the definition of the boundary is somewhat arbitrary.

There is some hint that in our results for the strong sequence $\xi = 0.18$, the four-shock TRR system appears immediately after transition to an irregular refraction. However, it is not resolved unequivocally, and in any event a TMR is certainly present when α_i increases by only a small further amount.

7. Concluding Remarks

In our calculations for the weak refraction sequence we used the same input data as Abd-El-Fattah and Henderson had measured in their experiments. This included the effects of gas contamination due to leakage and diffusion across the membrane, and also the inertia of the membrane. The object was to test the validity of the calculations by obtaining as precise a comparison with experiment as possible. We found that the membrane inertia made very little difference and we ignored it in our later calculations. However, our data for the wave angle α_t of the transmitted shock was sensitive to gas contamination, and to a lesser extent so was the wave velocity U_t data of this shock. None of the other data displayed such sensitivity, and was ascribed to the fact that α_t and U_t were measured for the CH_4 component which was significantly affected by contamination (Table 1) whereas the other data, χ, α_r, α_s, and so on, were measured for the CO_2 component which was very little affected by the contamination.

Our calculations were everywhere in reasonable agreement with experiment when gas contamination was taken into account, except for the α_t data when $\alpha_i > 60°$. There was there a discrepancy which was ascribed to the uncertainty of making accurate measurements of α_t due to the increasingly large curvature of the transmitted wave with increasing α_i. This uncertainty applied to both the experimental data and to measurements made from the contour plots.

The computations resolved the structure of the bound pre-cursor refraction (BPR), and revealed the presence of a fourth wave, which was an expansion and apparently centered on the refraction point. After transition to a free pre-cursor system, BPR $\rightarrow$ FPR, the transmitted/side shock pair were found to be smeared out in the region of the gas interface, called evanescent waves.

Similar effects were found in our calculations for stronger refraction and were ascribed to the same

causes. Our calculations displayed all the principle features found in experiment, such as local single Mach reflections, twin Mach reflections, free pre-cursor shocks, contact discontinuities, reflected expansion waves, and so on. We conclude that the code does provide a satisfactory representation of the refraction phenomena even though it ignores the effects of viscosity and three-dimensionality.

References

Abd-El-Fattah, A. M., Henderson, L. F. & Lozzi, A.1976 *J. Fluid Mech*, **76**, 157.

Abd-El-Fattah, A. M. & Henderson, L. F. 1978a *J. Fluid Mech.* **86**, 15.

Abd-El-Fattah, A. M. & Henderson, L. F. 1978b *J. Fluid Mech.* **89**, 79.

Berger, M. J. & Colella, P. 1989 *J. Comp. Phys.* **82**(1), 64.

Bitondo, D. 1950 *Inst. Aerophys., University of Toronto, UTIA Rept.* No. 7.

Colella, P., Ferguson, R. & Glaz, H. M. 1989 *Preprint in preparation.*

Colella, P. & Glaz, H. M. 1985 *J. Comp. Phys.* **59**, 264.

Colella, P. & Henderson, L. F. 1989 *J. Fluid Mech.* (In the press).

Colella, P. & Woodward, P. 1984 *J. Comp. Phys.* **54**, 174.

Glaz, H. M., Colella, P., Glass, I. I. & Deschambault, R. L. 1985 *Proc. Roy. Soc. Lond. A* **398**, 117.

Haas, J. F. & Sturtevant, B. 1987 *J. Fluid Mech.* **181**, 41.

Henderson, L. F. 1989 *J. Fluid Mech.* **198**, 365.

Hornung, H. G. & Taylor, J. R. 1982 *J. Fluid Mech.* **123**, 143.

Jahn, R. G. 1956 *J. Fluid Mech.* **1**, 457.

van Leer, R. G. 1979 *J. Comp. Phys.* **32**, 101.

von Neumann, J. 1943 In *Collected Works*, vol. 6, p. 1963. Pergamon.

Noh, W. F. & Woodward, P. 1976 *UCRL Preprint* No. 77651.

Smith, W. R. 1959 The Phys. of Fluids **2**, 533.

Figure Captions

Figure 1. Refraction of a normal shock wave at head-on incidence.

Figure 2. Regular and irregular shock refraction systems for a slow-fast CO_2/CH_4 gas interface, $n < 1$. (*a*) Regular refraction with reflected shock, RRR, $|Z_t| > |Z_i|$, $\alpha_t > \alpha_i$; (*b*) Regular refraction with reflected wave *a* Mach line degeneracy, $|Z_t| = |Z_i|$, $\alpha_t > \alpha_i = \alpha_{im}$; (*c*) Regular refraction with a reflected expansion wave, RRE, $|Z_t| < |Z_i|$, $\alpha_t > \alpha_i$; (*d*) Weak irregular refraction of the pre-cursor von Neumann type, FNR; (*e*) Intermediate irregular refraction of the twin regular reflection type, TRR; (*f*) Strong irregular refraction of the twin Mach reflection type TMR. *i*, incident shock; *t*, transmitted shock; *r*, reflected shock; *e*, reflected expansion wave, *k*, modified incident shock; *n* Mach shock; *s*, side shock; *m* gas interface; I, region of undisturbed CO_2; II, region of undisturbed CH_4; *MW*, Mach line; *cd*, contact discontinuity; *O* origin where *i* first encountered gas interface.

Figure 3. Polar diagrams for a weak shock refraction sequence, $\xi_i = 0.78$, at a pure CO_2/CH_4 gas interface. M_{oi}, M_{ot}, M_{or}, free stream Mach numbers, upstream and relative to the *i*, *t*, and *r* shocks; (ϵ_1, λ_1, λ_2) solutions of the von Neumann regular refraction theory; *D*, disturbed gas interface; A_1, intersection point of the primary polars (i,t). For other symbols see the caption to Figure 2. (a) Regular refraction with a reflected expansion *e*, (RRE); $|Z_t| < |Z_i|$; $\alpha_i = 27°$; (b) Regular refraction with a degenerate reflection, $|Z_t| = |Z_i|$; $R = 0$, $T = 1$, the condition for total energy transmission; $\alpha_i = \alpha_{im} = 32.0592°$ is the angle of intromission; (c) Regular refraction with a reflected shock *r*, (RRR); $|Z_t| > |Z_i|$; $\alpha_i = 33.27°$; (d) Condition of RRR at the shock critical angle $\alpha_{sc} \approx 34.4885°$; (e) Irregular refraction for $\alpha_i > \alpha_{sc}$, called a bound pre-cursor refraction BPR; (f) Irregular refraction after violation of refraction law, called a free pre-cursor refraction; *s* and *t* are evanescent waves; (g) Irregular refraction called a free pre-cursor von Neumann refraction (FNR).

Figure 4. Contour plots of log *P* for a weak shock refraction sequence $\xi_i = 0.78$, at a pure CO_2/CH_4 gas interface. The line running diagonally from upper left to lower right represents the initial, undisturbed gas interface. It is drawn here for reference only and does not represent a contour line of the pressure. (a) $\alpha_i = 27°$, RRE; (b) Total transmission at angle of intromission, $\alpha_i = \alpha_{im} = 32.0592°$; (c) $\alpha_i = 33.27°$, RRR; (d) RRR $\rightleftharpoons$ BPR, $\lambda_1 \equiv \lambda_2$, at the shock critical angle $\alpha_{sc} \approx 34.4885°$; (e) $\alpha_i = 38°$, BPR; (f) $\alpha_i = 43°$, FPR; (g) $\alpha_i = 49°$, FPR; (h) $\alpha_i = 65°$, FPR;

Figure 5. (Plates 1 and 2) Schlieren photograph and color graphics for a weak irregular shock refraction, TNR, $\xi_i = 0.78$, $\alpha_i = 60°$, at a CO_2/CH_4 gas interface. Note that the schlieren photograph was taken during the experiment so the experimental artifacts of the polymer membrane and gas contamination are present. The color graphics are for the pure gas and without the membrane.

Figure 6. Comparison of angles measured from the numerical contour plots with those measured from the schlieren photographs from the experiments, for the CO_2/CH_4 gas interface, for a weak shock refraction sequence, $\xi_i = 0.78$. •, experimental data for α_t for regular refraction; $\odot$, experimental data for α_t for irregular refraction; $\triangle$, experimental data for the reflected wave angle α_e, or, α_r in regular refraction; $\triangledown$, experimental data for the reflected wave angle in irregular refraction; $\diamondsuit$, experimental data for the side shock angle α_s; $\bigcirc$, experimental data for the trajectory path angle χ; χ, angle measured from the numerical plots for the contaminated gas interface; +, angles measured from the numerical plots for the pure gas interface; $\dotplus$, indication of experimental error. (Experimental data from Abd-El-Fattah and Henderson 1978b.)

Figure 7. Comparison for the wave speed ration U_t/U_i measured from the numerical contour plots with those measured from the schlieren photographs from the experiments, for the CO_2/CH_4 gas interface for a weak shock refraction sequence, $\xi_i = 0.78$. (Experimental data from Abd-El-Fattah and Henderson 1978b.) $\odot$, experimental data; for other symbols see caption to Figure 6.

Figure 8. Comparison of the wave speed ration U_t/U_i measured from the numerical contour plots with those measured from the schlieren photographs from the experiment for the CO_2/CH_4 gas interface for a

strong shock sequence. $\xi_i = 0.18$. For other information see the caption to Figure 7.

Figure 9. Contour plots of log P and log ρ for a strong shock refraction sequence, $\xi_i = 0.18$, at a pure CO_2/CH_4 gas interface.

Figure 10. (Plates 3 and 4) Schlieren photograph and color graphics plot for a strong shock irregular refraction, TMR, $\xi_i = 0.18$, $\alpha_i = 66°$, at a CO_2/CH_4 gas interface. See also note to the caption of Figure 5.

Figure 11. Polar diagrams for a strong shock refraction sequence, $\xi_i = 0.18$ at a pure CO_2/CH_4 gas interface. (a) RRE, ϵ_n solution at $\alpha_i = 30°$; (b) RRE, ϵ_1 solution at $\alpha_i = \alpha_{sc} = 35.95°$. Note that ϵ_1 is not a continuation of either the λ_1, or λ_2 solutions, therefore the shock critical angle for $\lambda_1 \equiv \lambda_2$ is irrelevant for transition to irregular refraction in this case; (c) RRE, at $\alpha_i = 37°$; note there are now two RRE solutions, ϵ_1 and ϵ_2; the ϵ_1 solution is observed in experiments; (d) RRE, at the relevant shock critical angle, $\epsilon_1 \equiv \epsilon_2$, $\alpha_1 = \alpha_{sc} = 46.294°$: transition condition for RRE $\rightleftharpoons$ TMR; (e) Twin-Mach-reflection-refraction (TMR) at $\alpha_i = 66° > \alpha_{s_c}$.

Figure 12. Comparison of angles measured from the numerical contour plots with those measured from the schlieren photographs from the experiments, for the CO_2/CH_4 gas interface, for a strong shock refraction sequence, $\xi_i = 0.18$. For the definition of the symbols see the caption to Figure 6.

Figure 13. (Plates 5 and 6) Schlieren photograph and color graphics for an intermediate shock irregular refraction, TRR, $\xi_i = 0.53$, $\alpha_i = 50°$, at a CO_2/CH_4 gas interface. See also the caption to Figure 5.

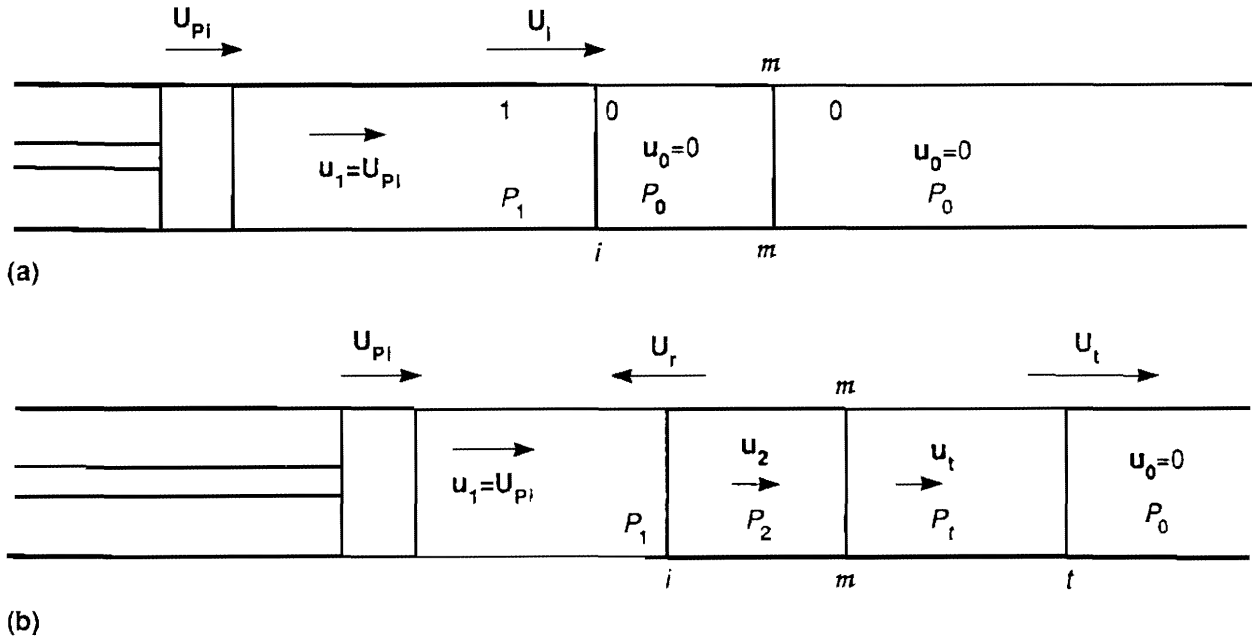

Figure 1. Refraction of a normal shock wave *i* at zero angle of incidence at a plane interface between two media: (a) before refraction; (b) after refraction.

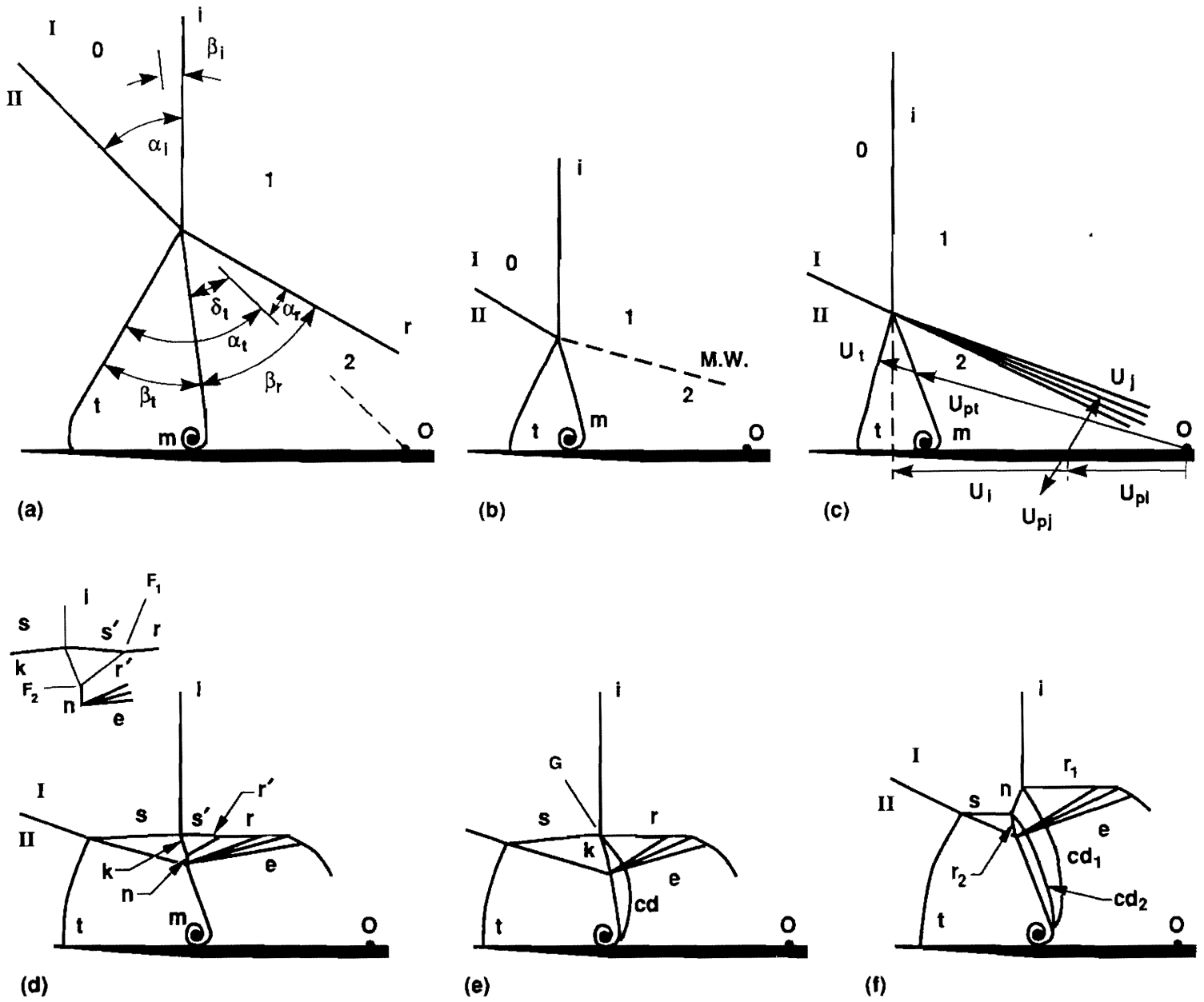
I
0
i
β_i
II
α_i
1
δ_t
α_r
r
α_t
2
t
β_t
β_r
m
O
(a)
i
I 0
II
1
M.W.
2
t
m
O
(b)
i
0
1
I
II
U_t
2
U_j
U_{pt}
t
m
O
U_i
U_{pj}
U_{pl}
(c)
F_1
i
s
s′
r
k
r′
F_2
n
e
i
I
s
s′
r′
r
II
k
e
n
t
m
O
(d)
i
G
s
r
k
e
cd
t
O
(e)
i
I
r_1
n
II
s
e
r_2
cd_1
cd_2
t
O
(f)

Figure 2

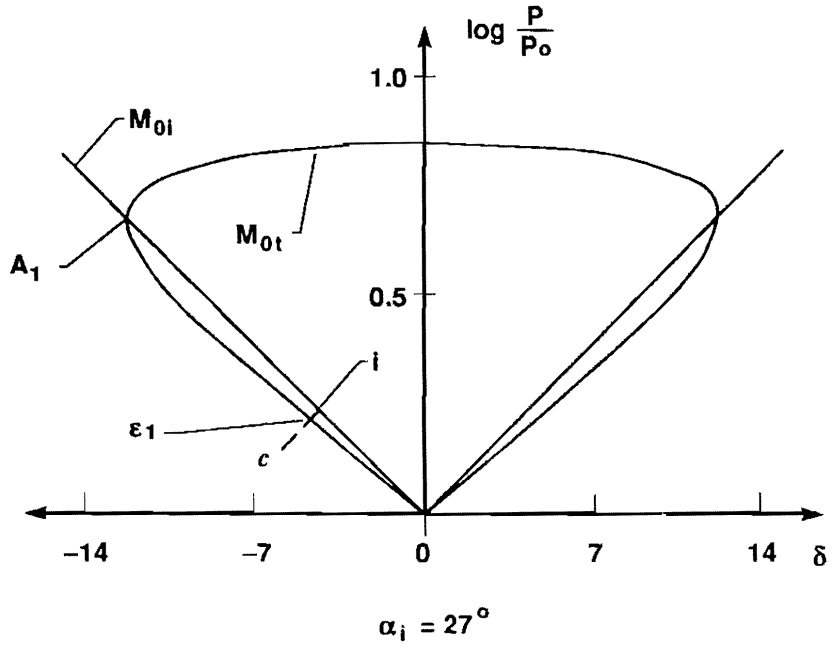
log P/Po
1.0
0.5
M0i
M0t
A1
i
ε1
c
-14
-7
0
7
14
δ
αi = 27°

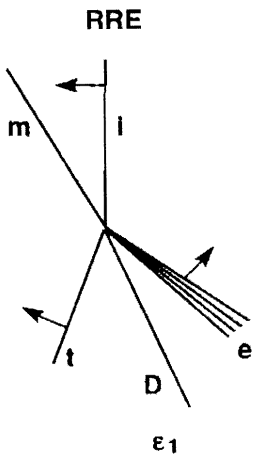
RRE
m
i
t
D
e
ε1

Fig 3a

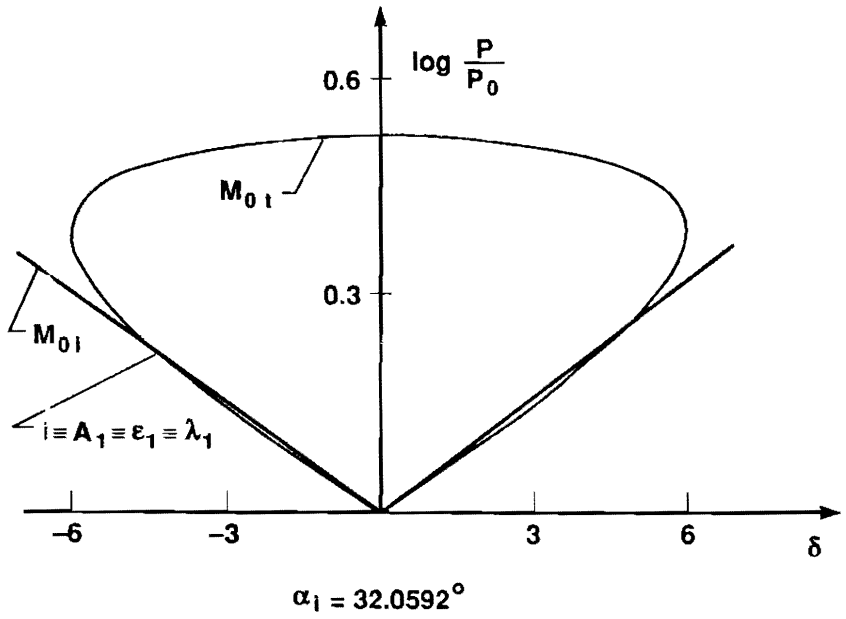
log P/P0
0.6
0.3
M0 t
M0 i
i ≡ A1 ≡ ε1 ≡ λ1
-6
-3
3
6
δ
αi = 32.0592°

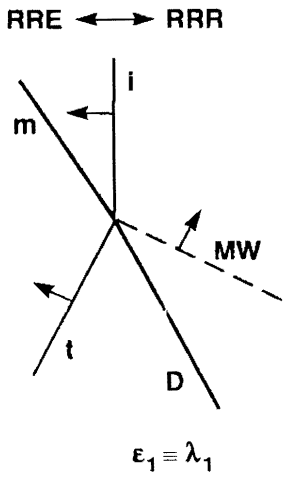
RRE ⟷ RRR
i
m
MW
t
D
ε1 ≡ λ1

Fig 3b

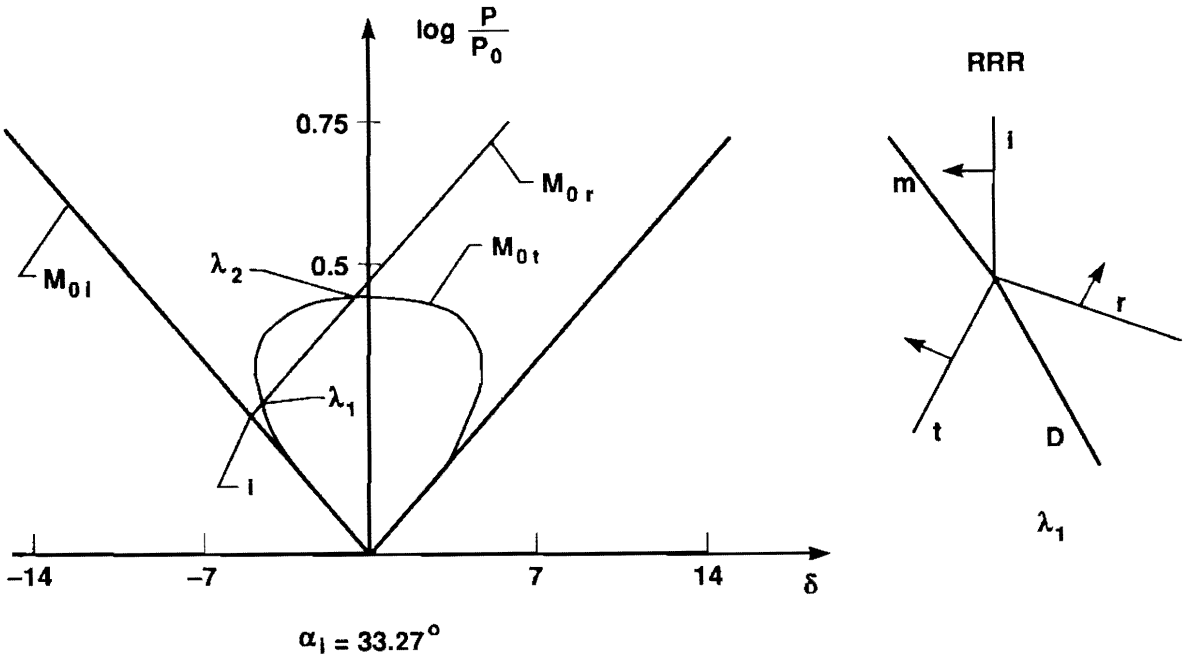

$\alpha_i = 33.27°$

Fig 3c

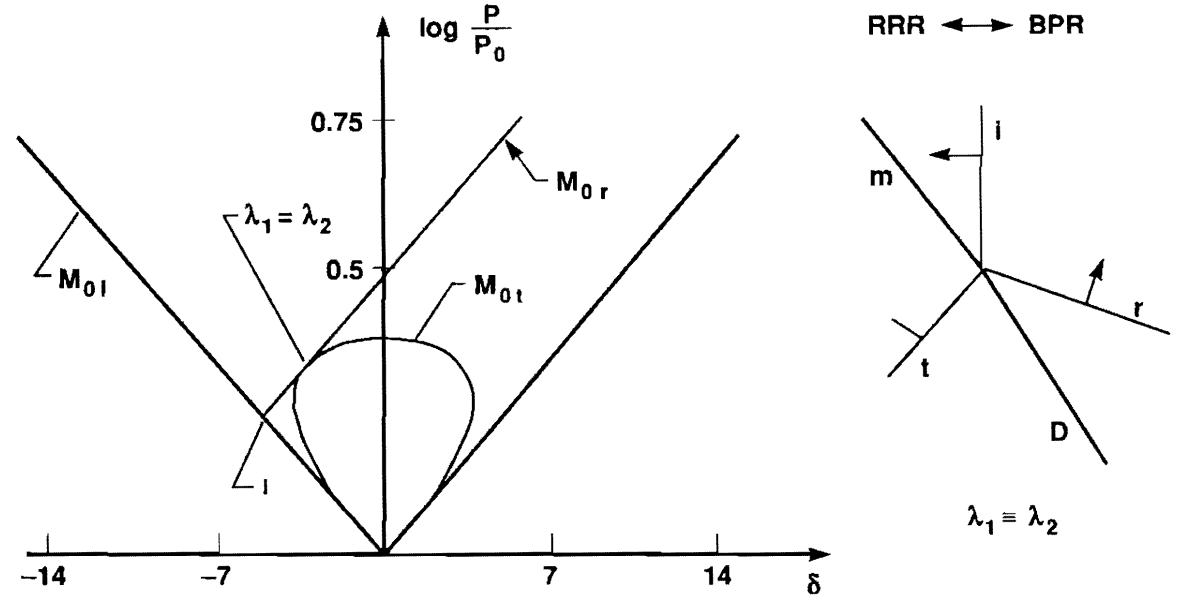

$\alpha_i = 34.4885°$

Fig 3d

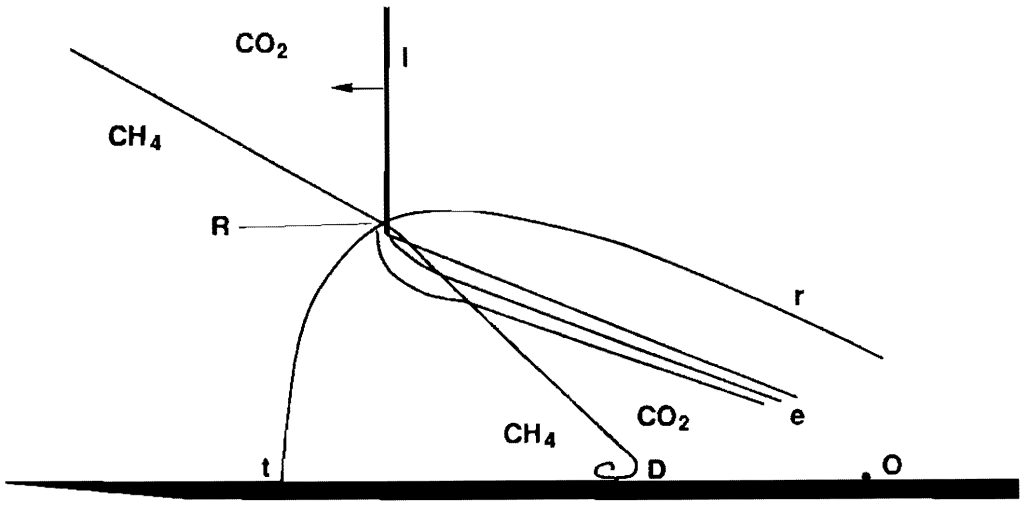

BPR

Fig 3e

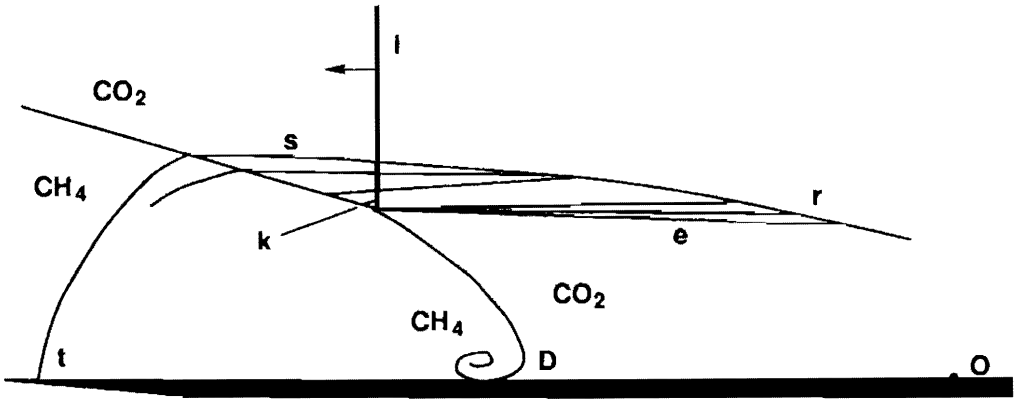

FPR

Fig 3f

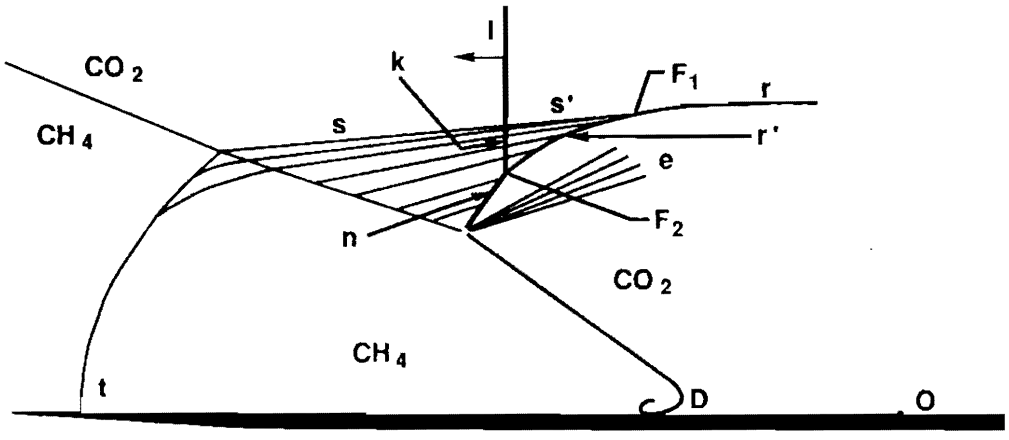

FNR

Fig 3g

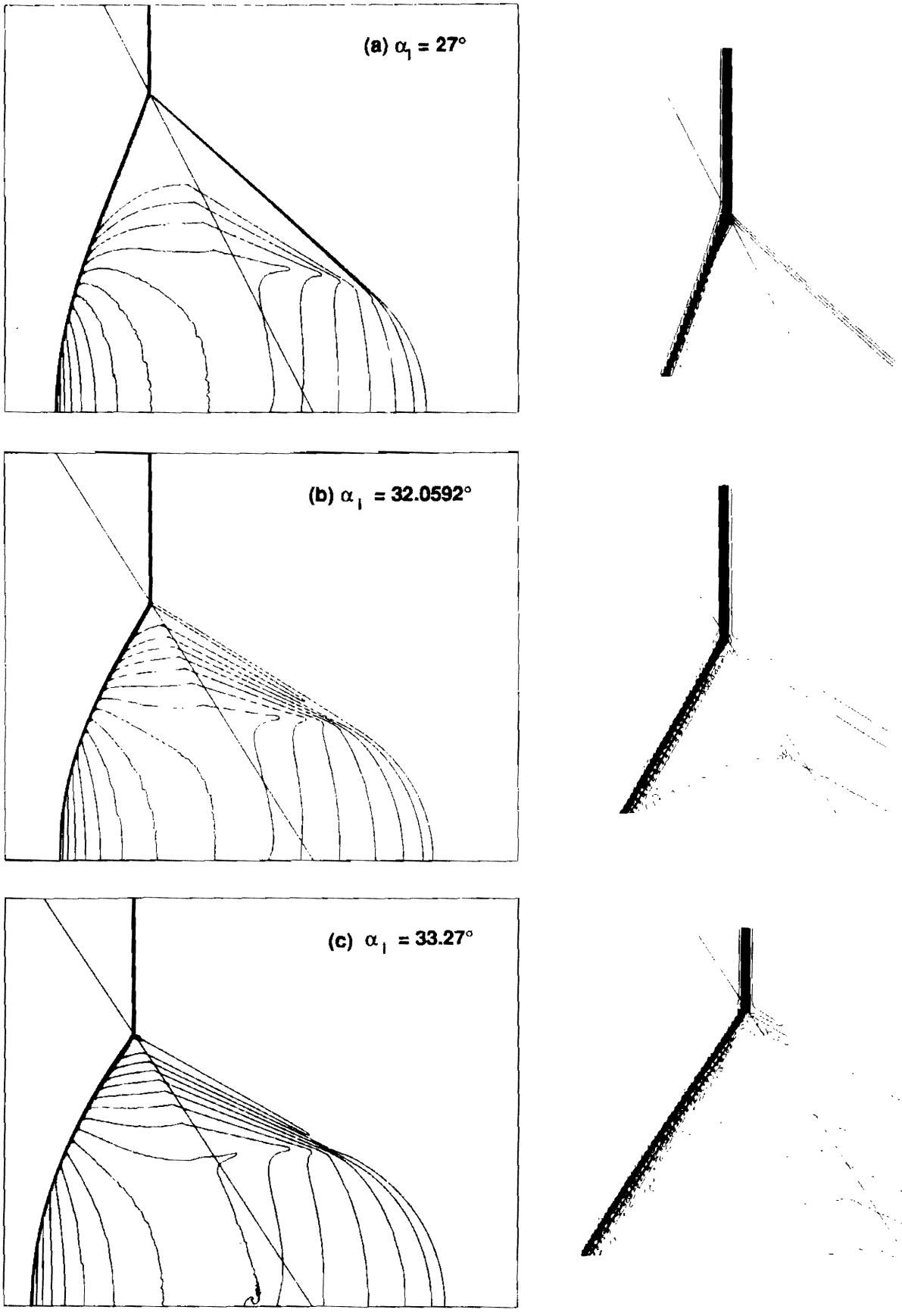

Figure 4

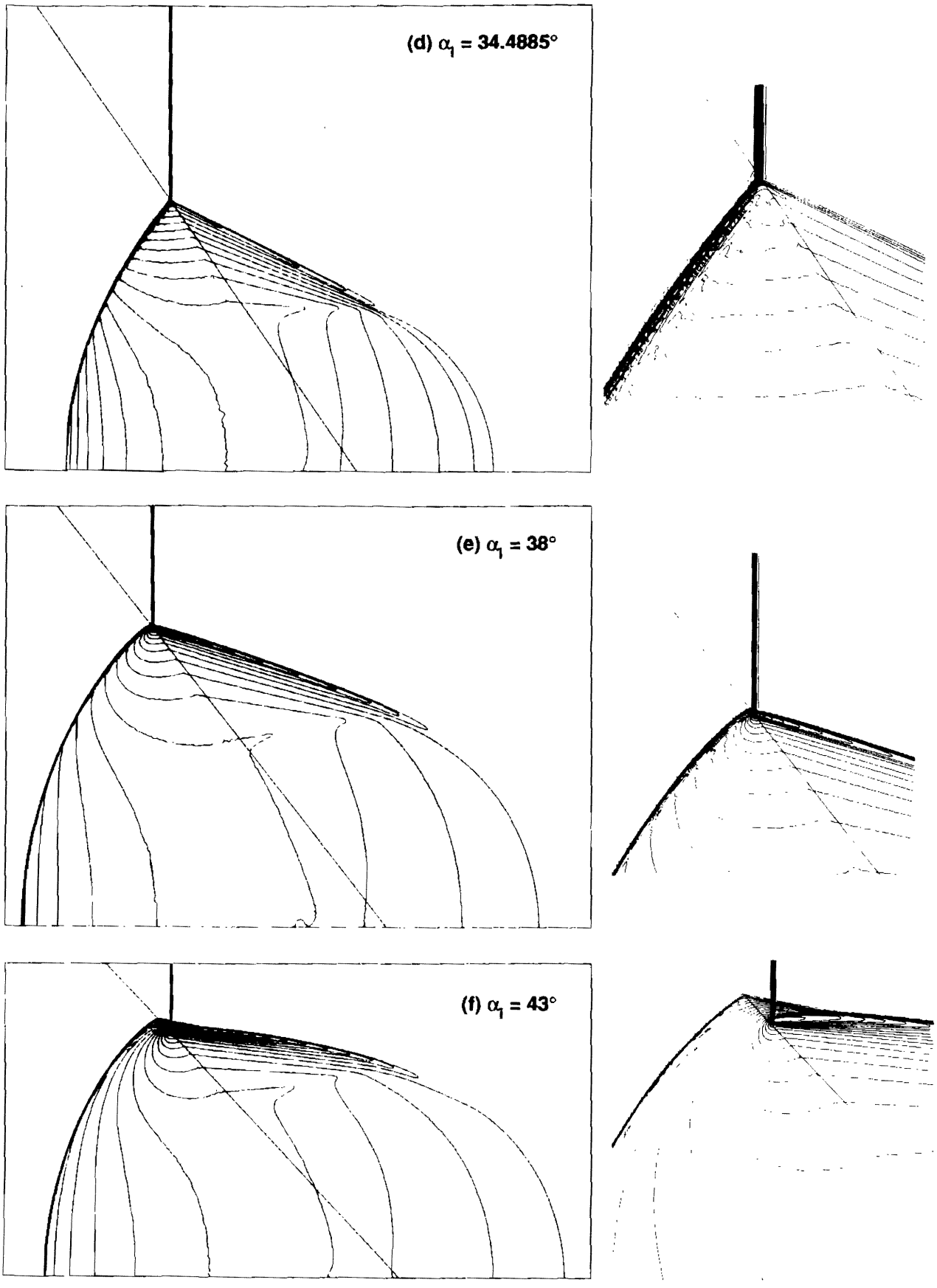

Figure 4

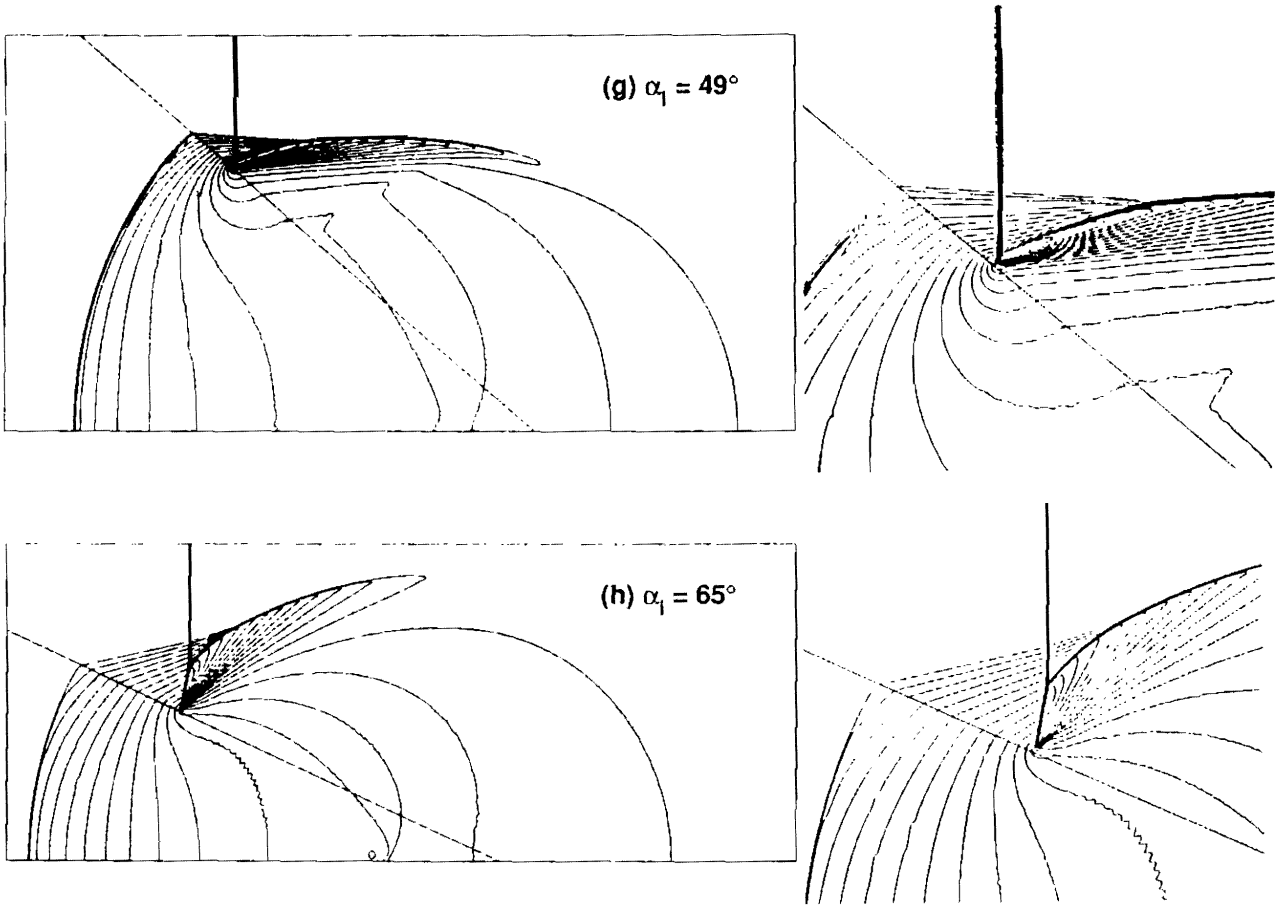

Figure 4

(a) Schlieren Photo

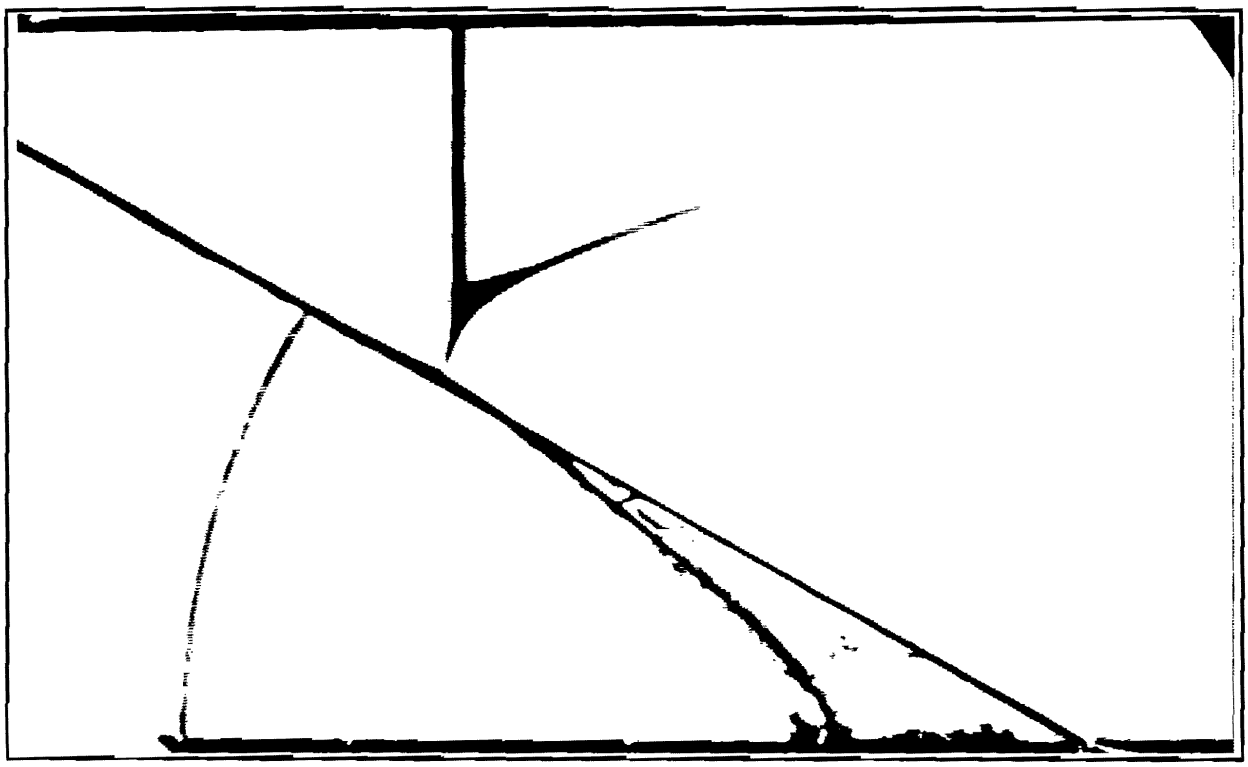

(b) div $\hat{u}$

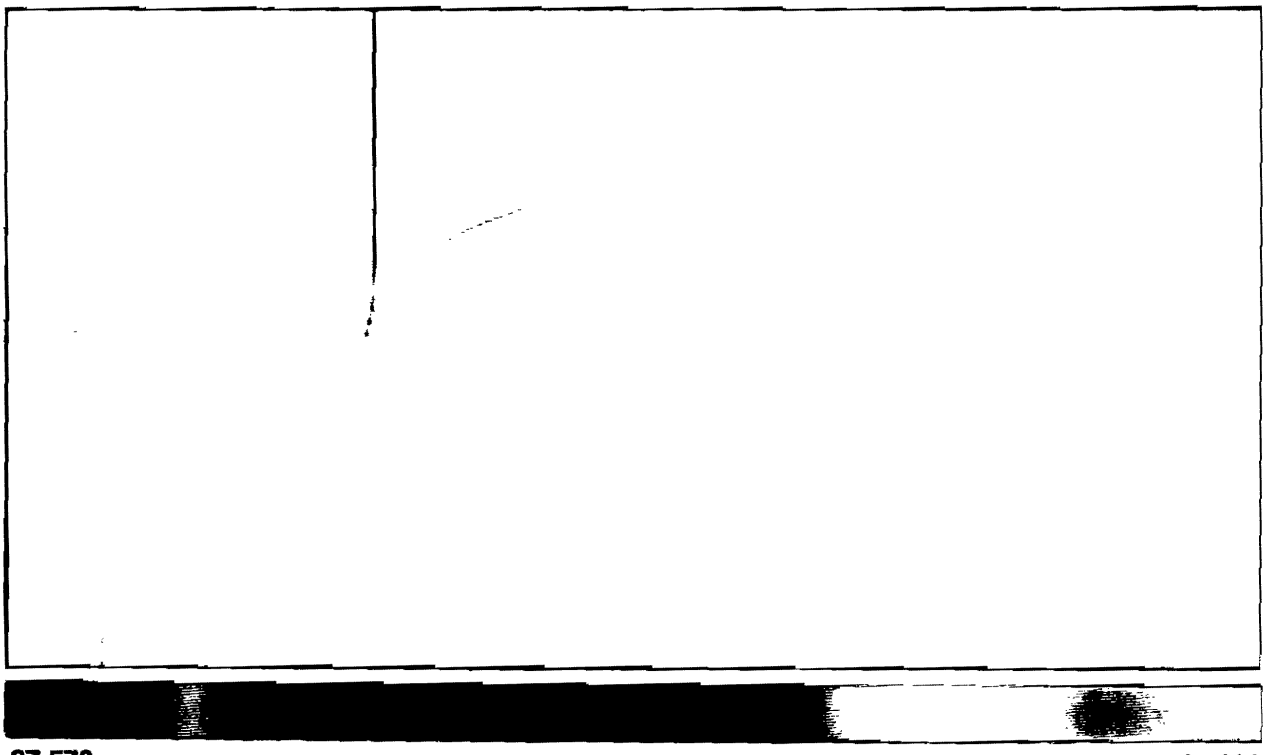

-87.572 31.228

Fig. 5

MI014-U-6764-5

(c) Log ρ

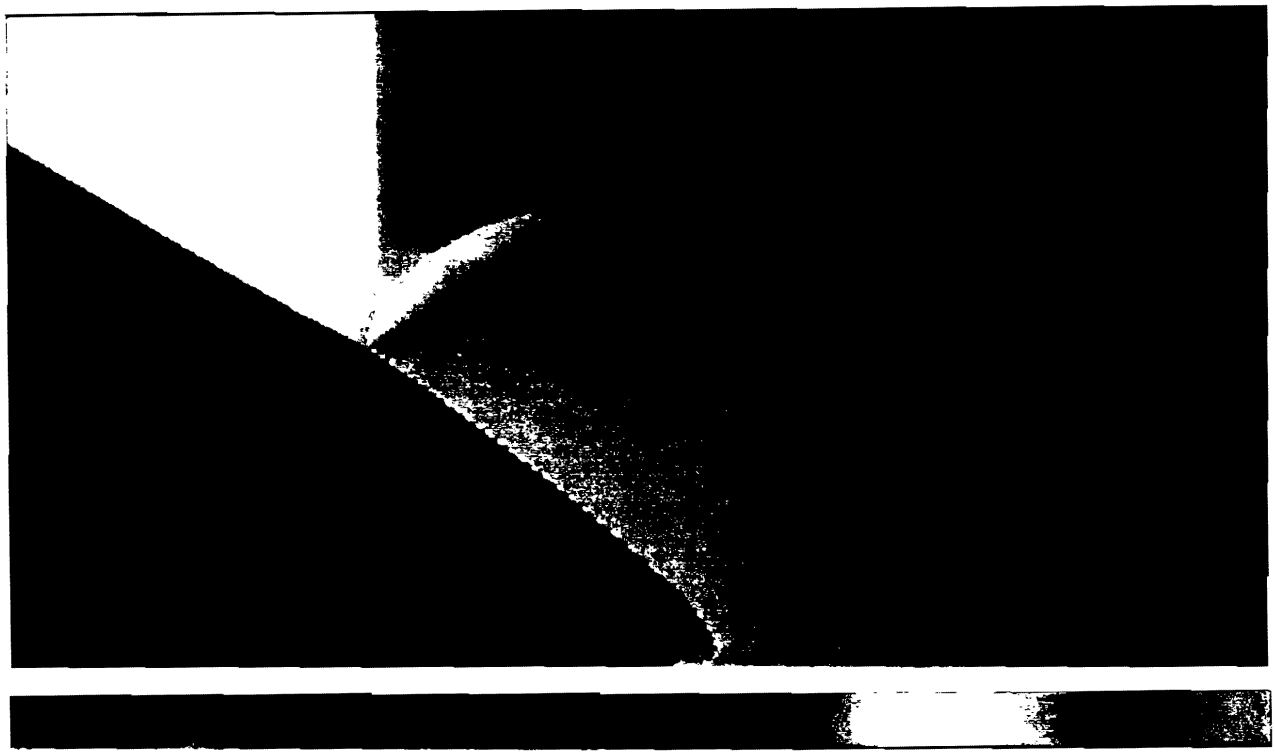

-0.328 -0.231

(d) Log p

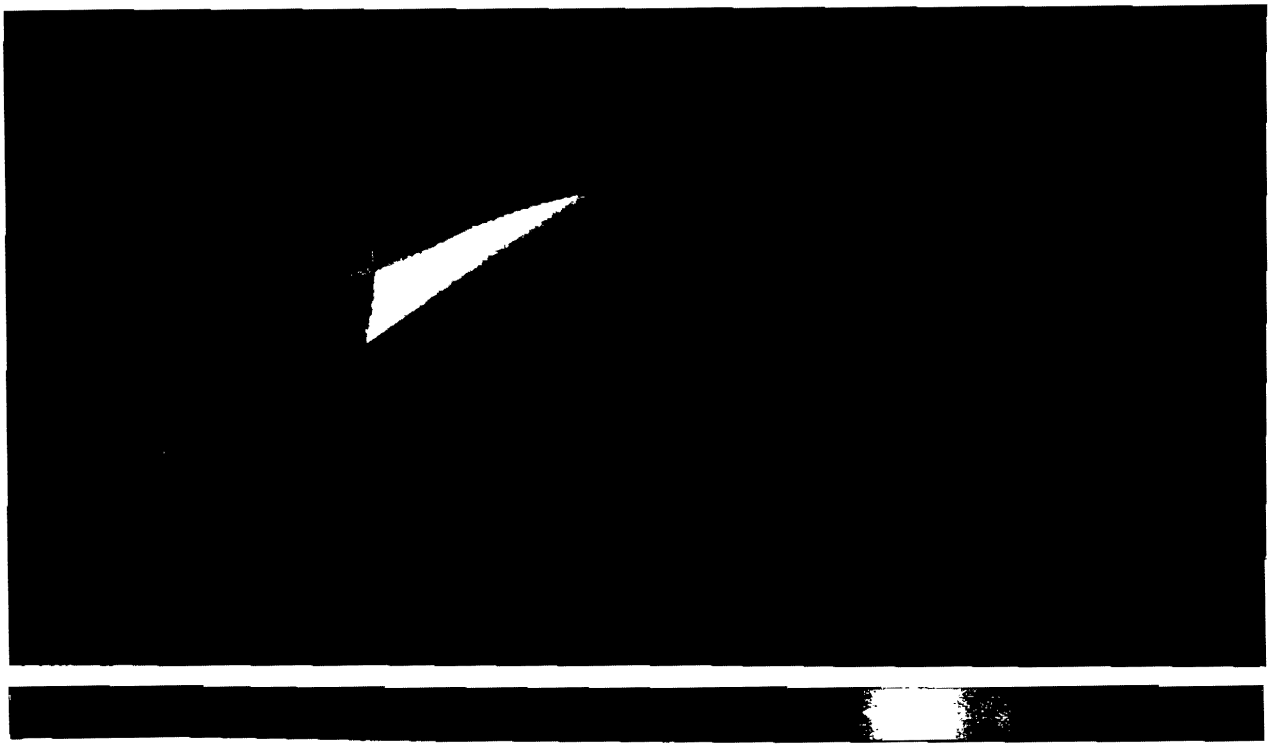

0.000 0.220

Fig. 5

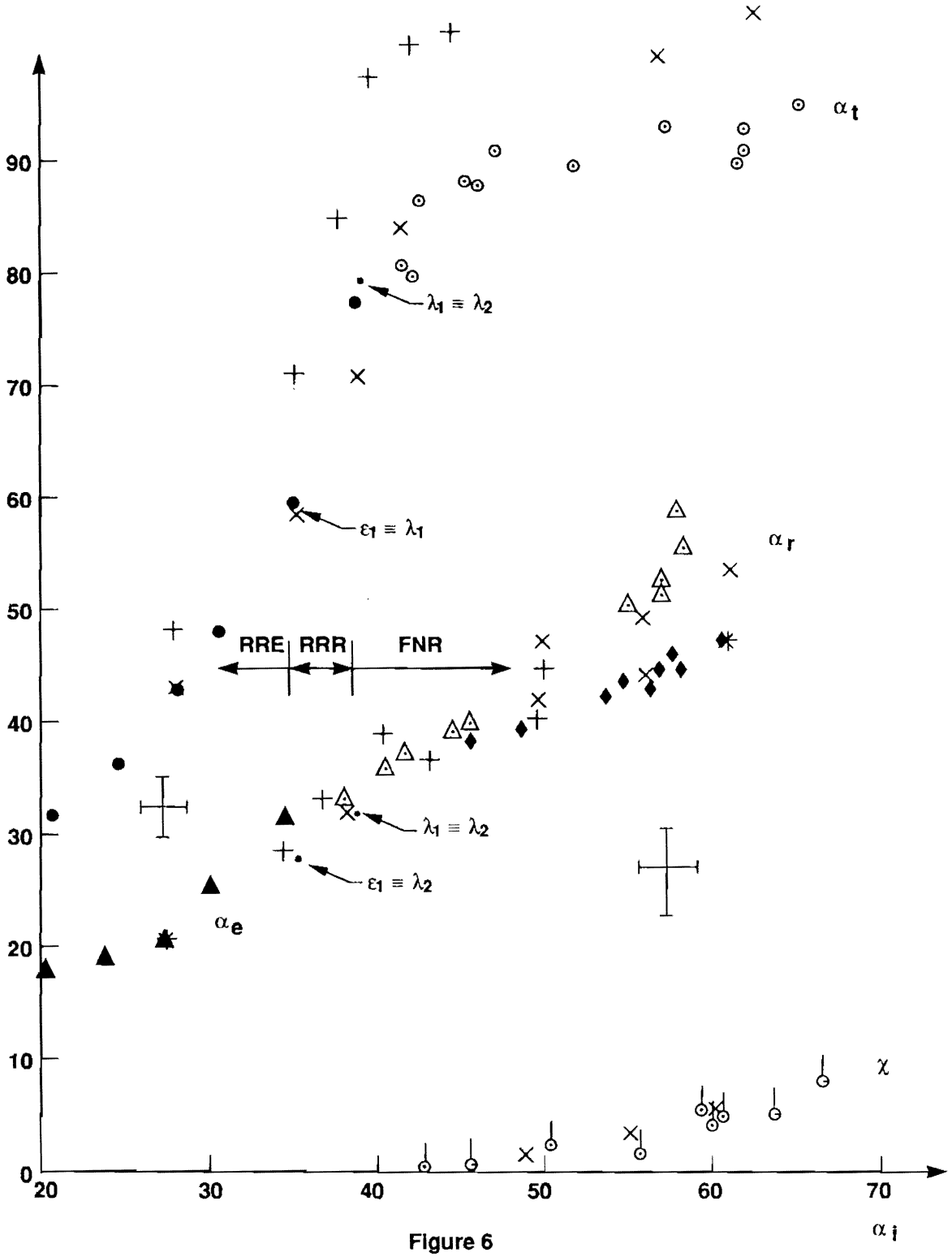
90
80
70
60
50
40
30
20
10
0
20
30
40
50
60
70
α_j
α_t
α_r
α_e
χ
$\lambda_1 \equiv \lambda_2$
$\varepsilon_1 \equiv \lambda_1$
$\lambda_1 \equiv \lambda_2$
$\varepsilon_1 \equiv \lambda_2$
RRE
RRR
FNR

Figure 6

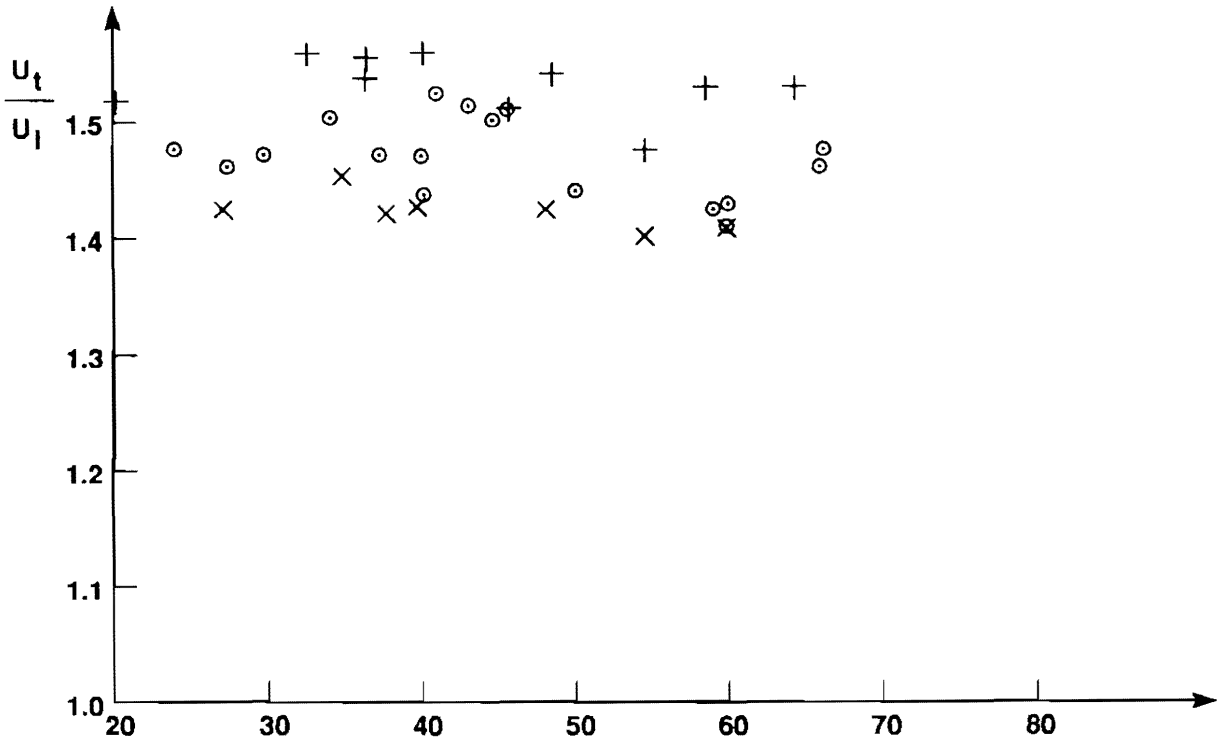

Figure 7

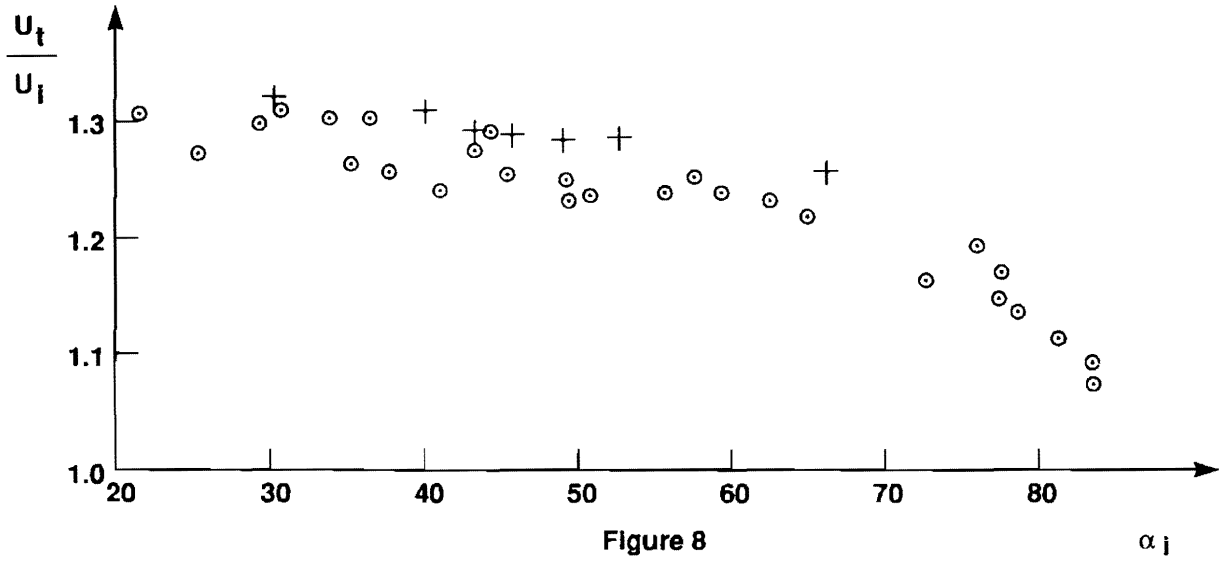

Figure 8

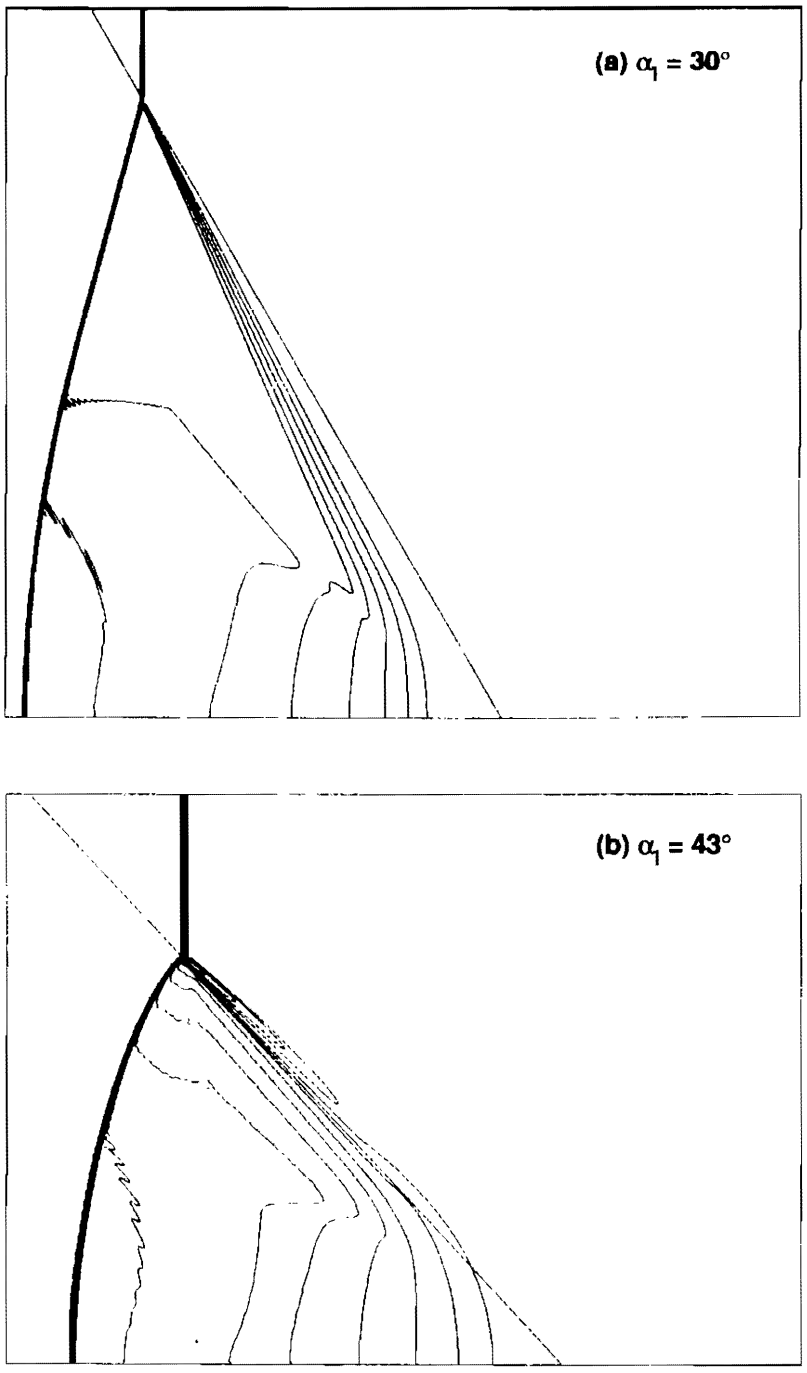

Figure 9

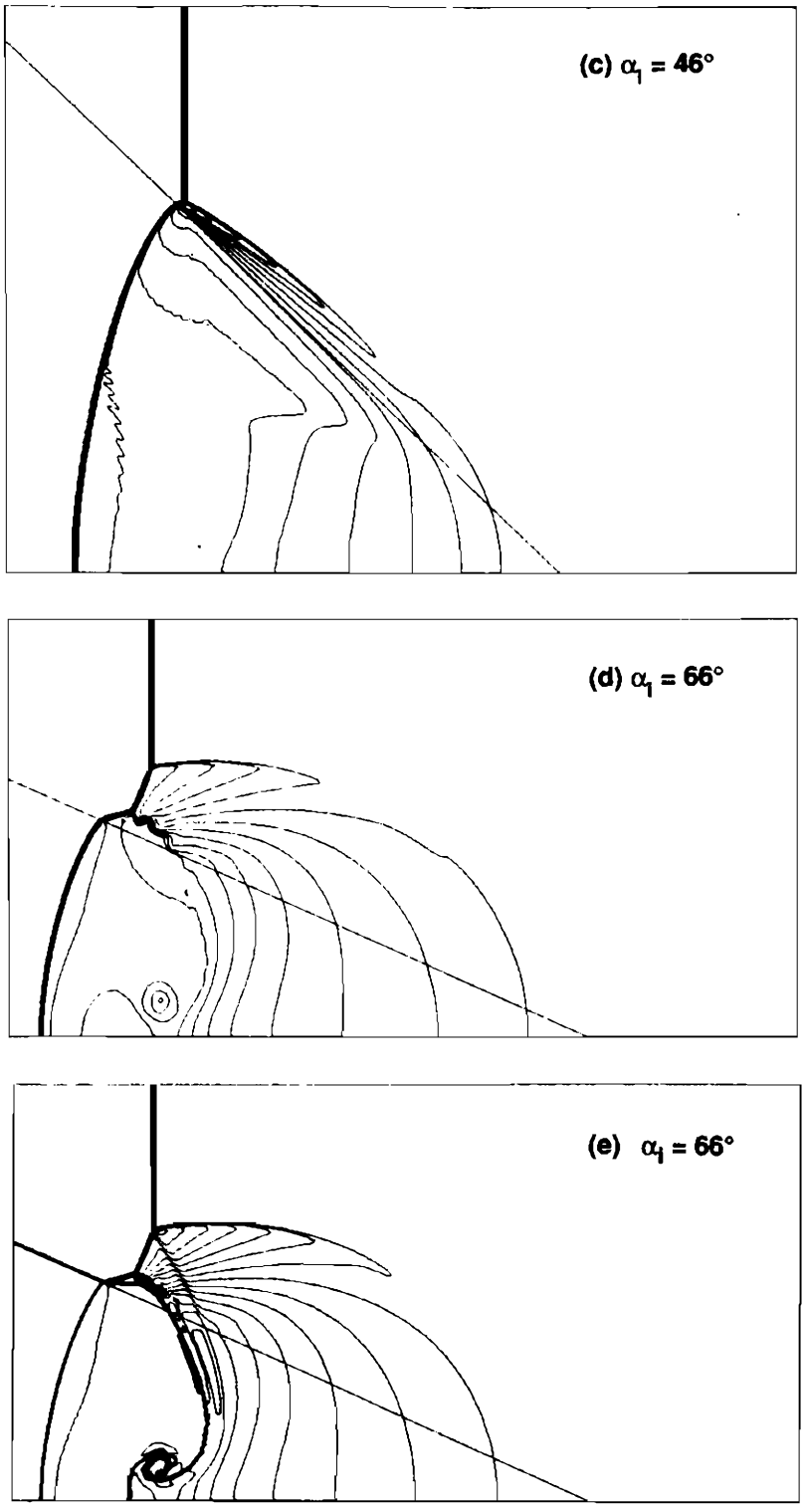

Figure 9

(a) Schlieren Photo

(b) div $\hat{u}$

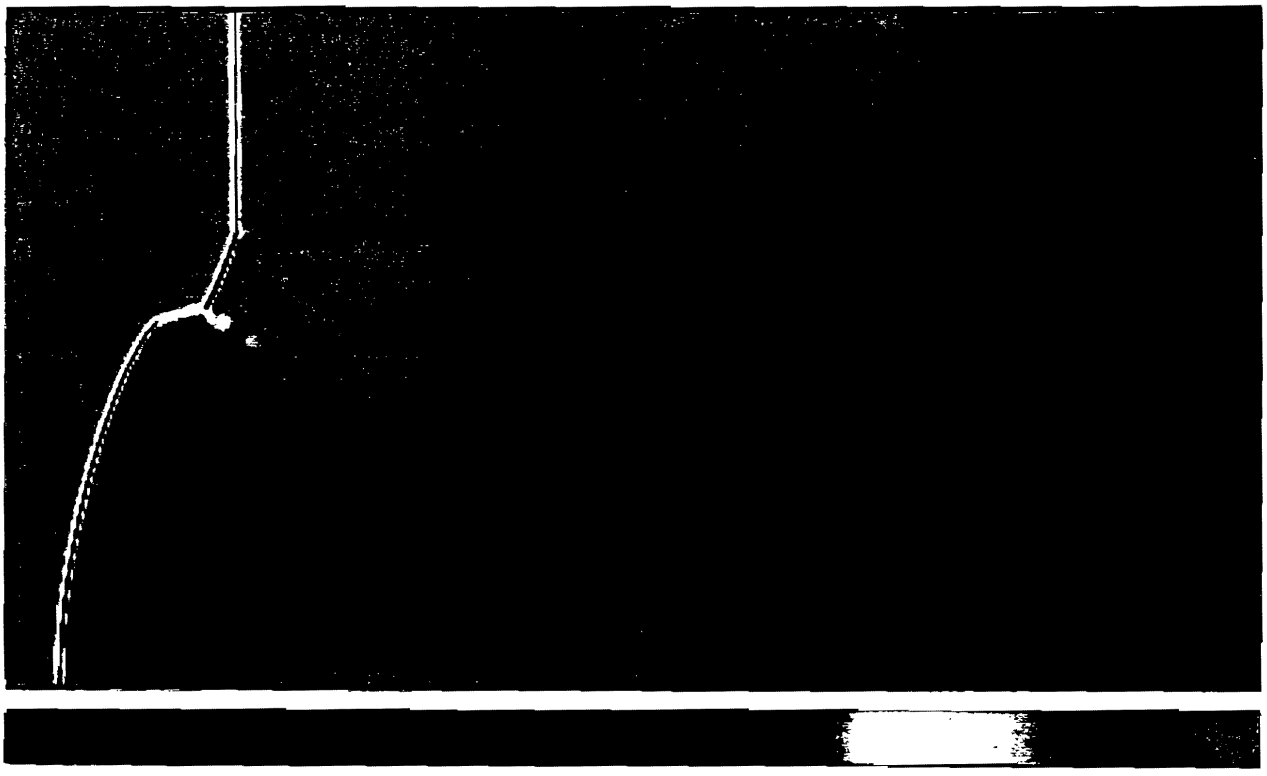

-577.037 70.604

Fig. 10

(c) Log ρ

-0.328 0.765

(d) Log p

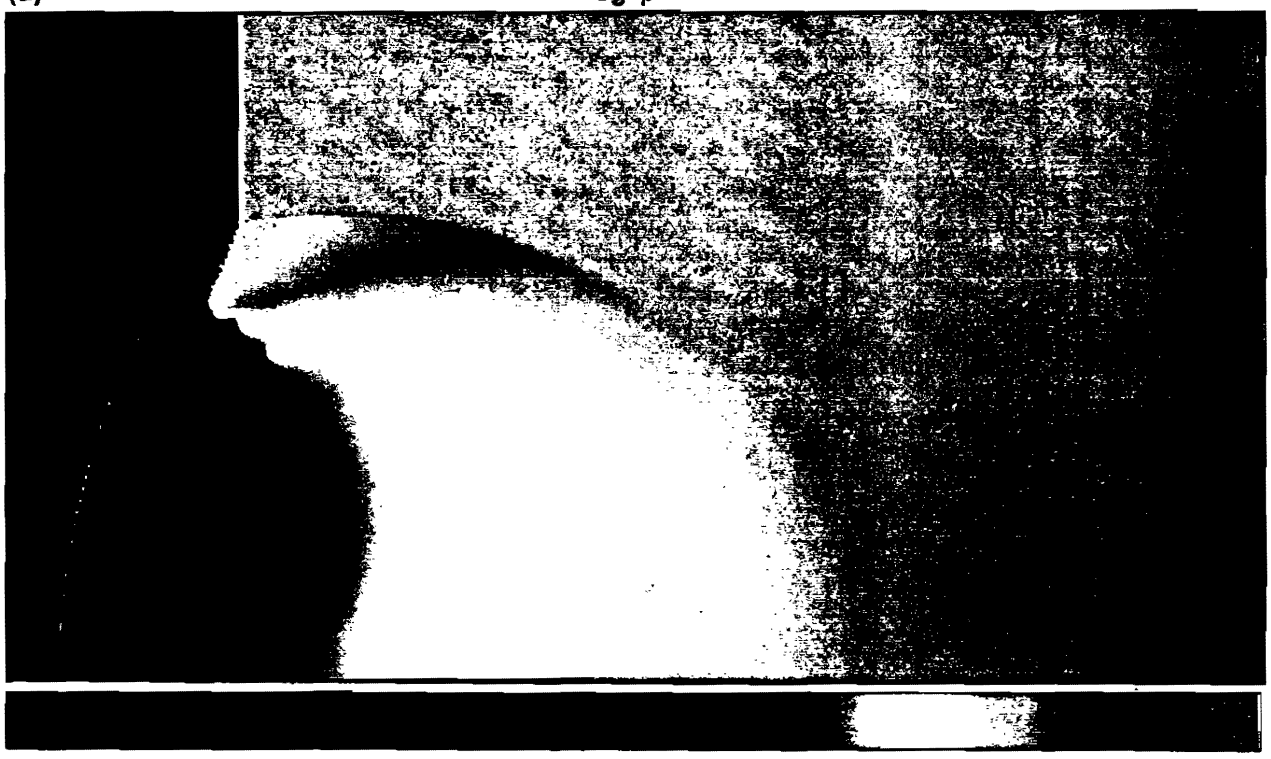

0.000 0.804

Fig. 10

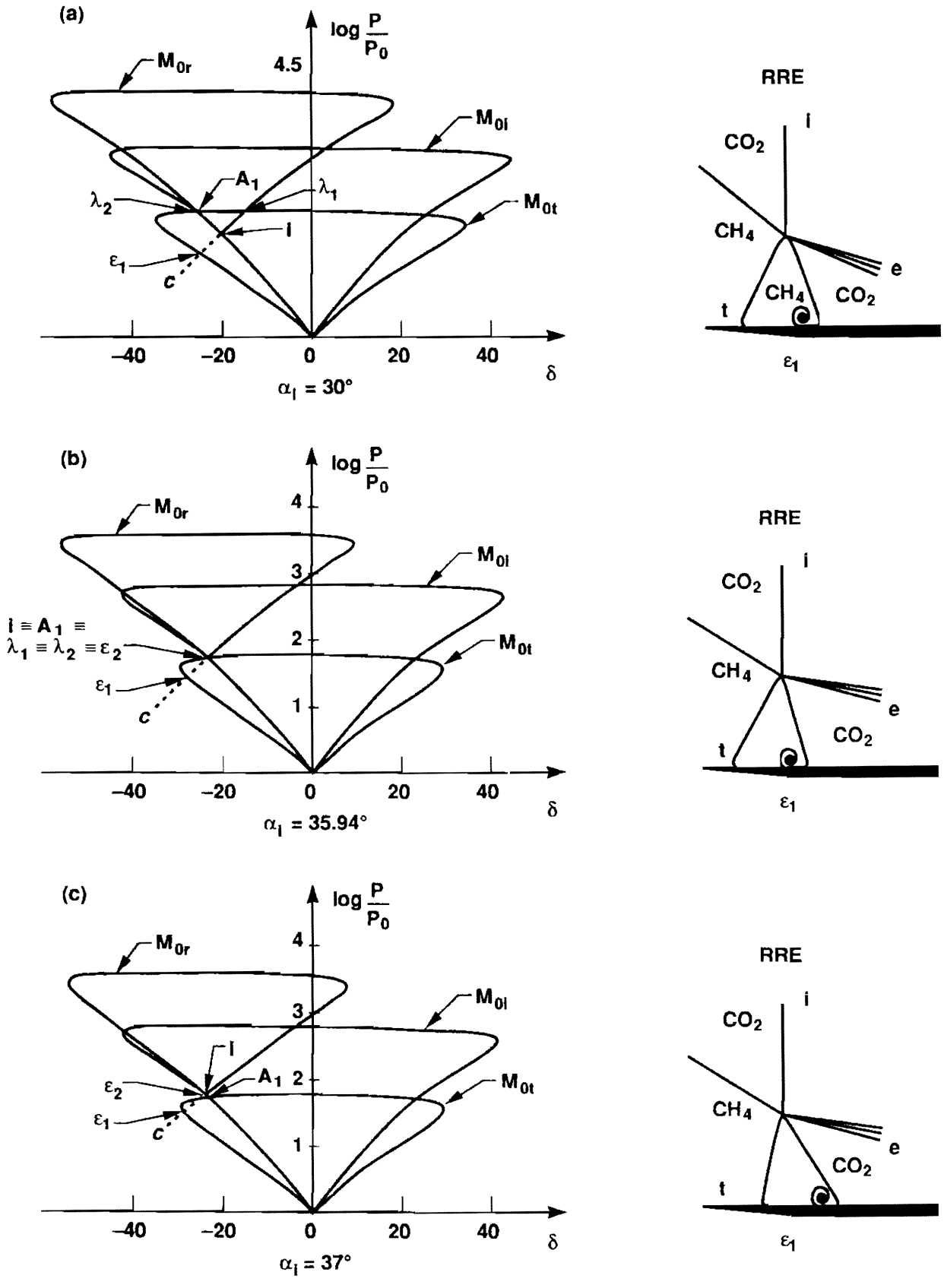

Figure 11

QT-KC-U-6764-11a,b,c

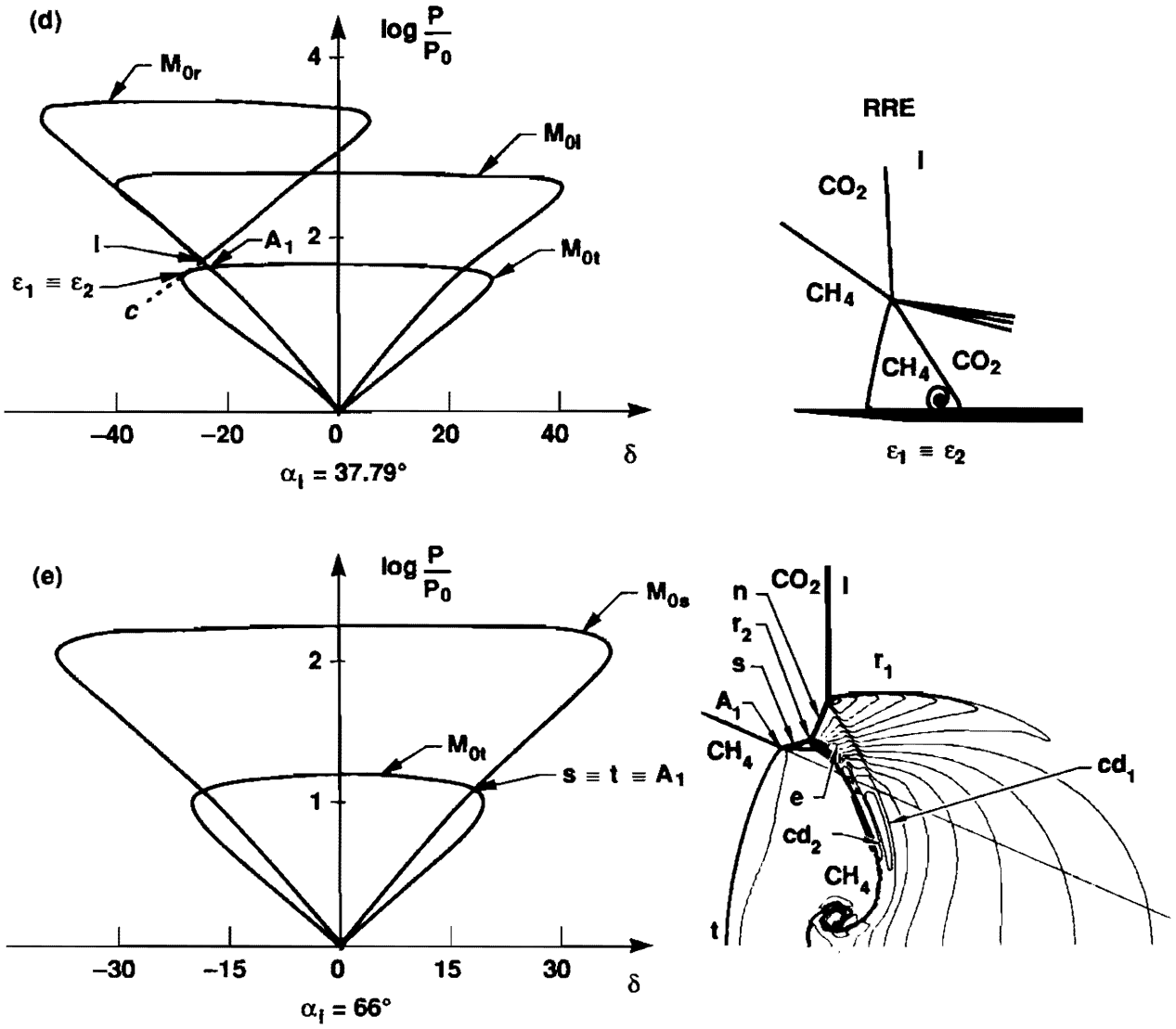
(d)
log P/P0
4
M0r
M0l
M0t
I
A1
2
ε1 ≡ ε2
c
–40
–20
0
20
40
δ
αI = 37.79°
RRE
I
CO2
CH4
CH4
CO2
ε1 ≡ ε2
(e)
log P/P0
M0s
2
M0t
s ≡ t ≡ A1
1
–30
–15
0
15
30
δ
αI = 66°
n
CO2
I
r2
s
r1
A1
CH4
cd1
e
cd2
CH4
t

Figure 11

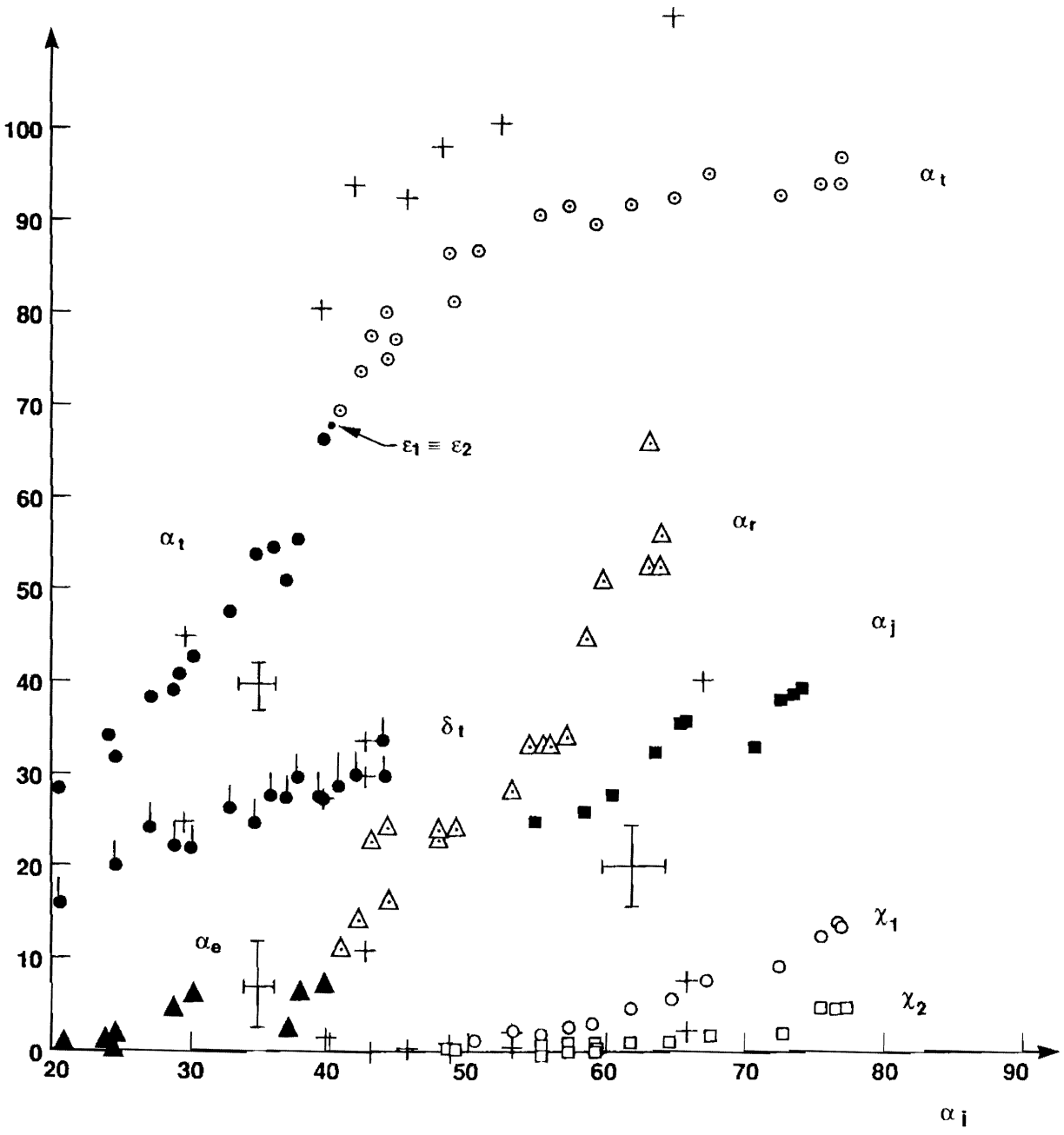
100
90
80
70
60
50
40
30
20
10
0
20
30
40
50
60
70
80
90
α_i
α_t
$\varepsilon_1 \equiv \varepsilon_2$
α_t
α_r
α_j
δ_t
α_e
χ_1
χ_2

Figure 12

(a) Schlieren Photo

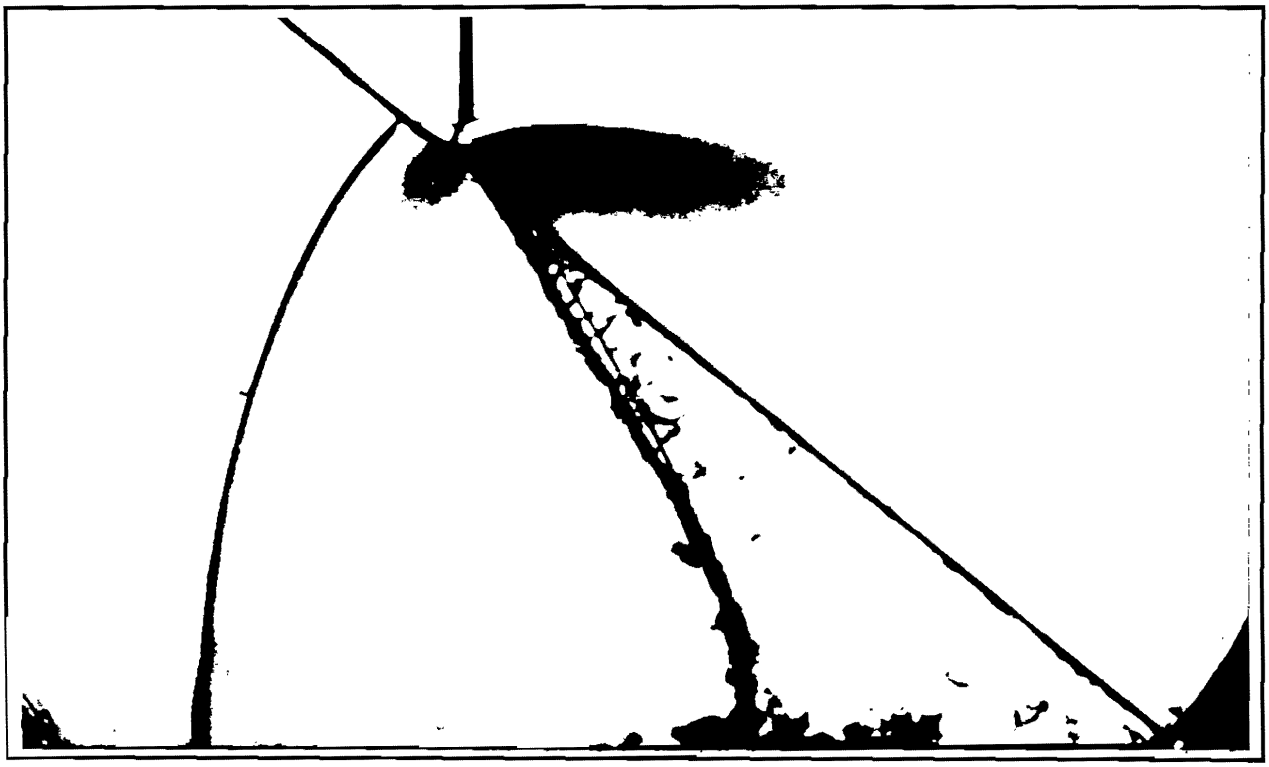

(b) div $\hat{u}$

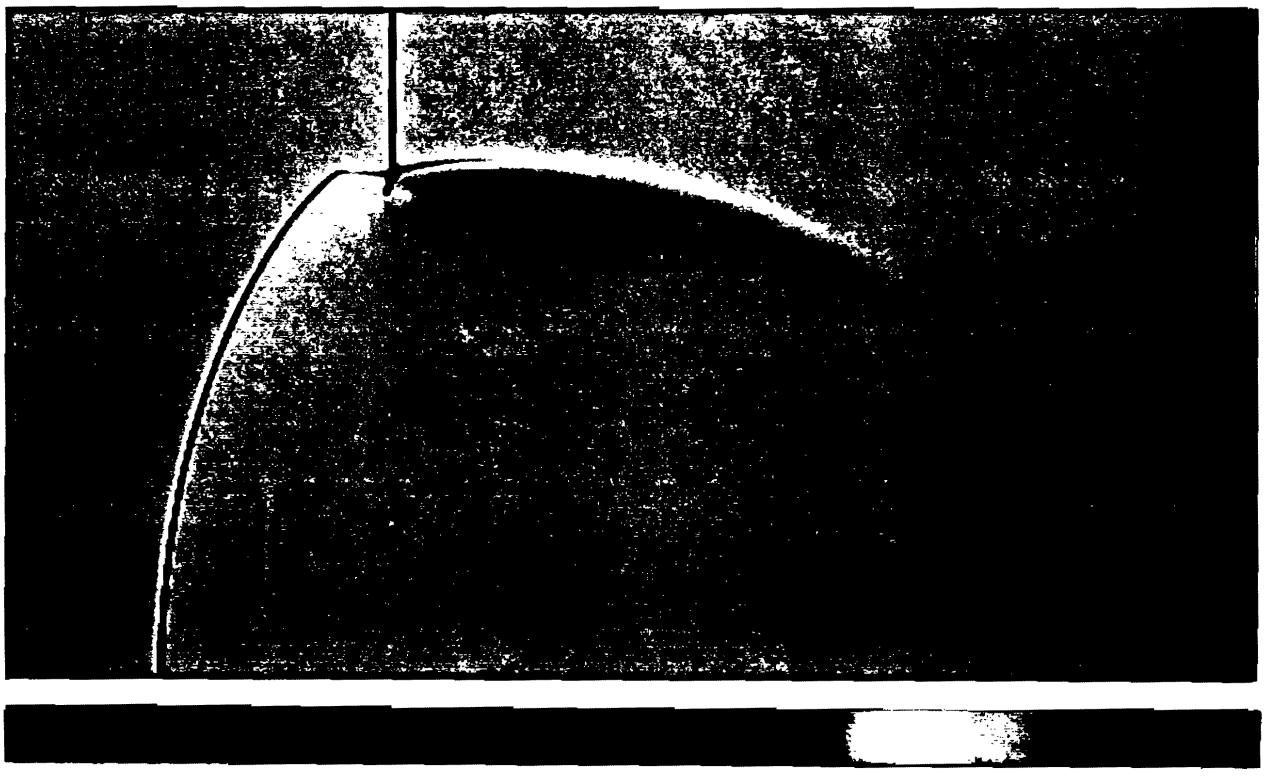

-163.393 36.286

Fig. 13

MI014-U-6764-13

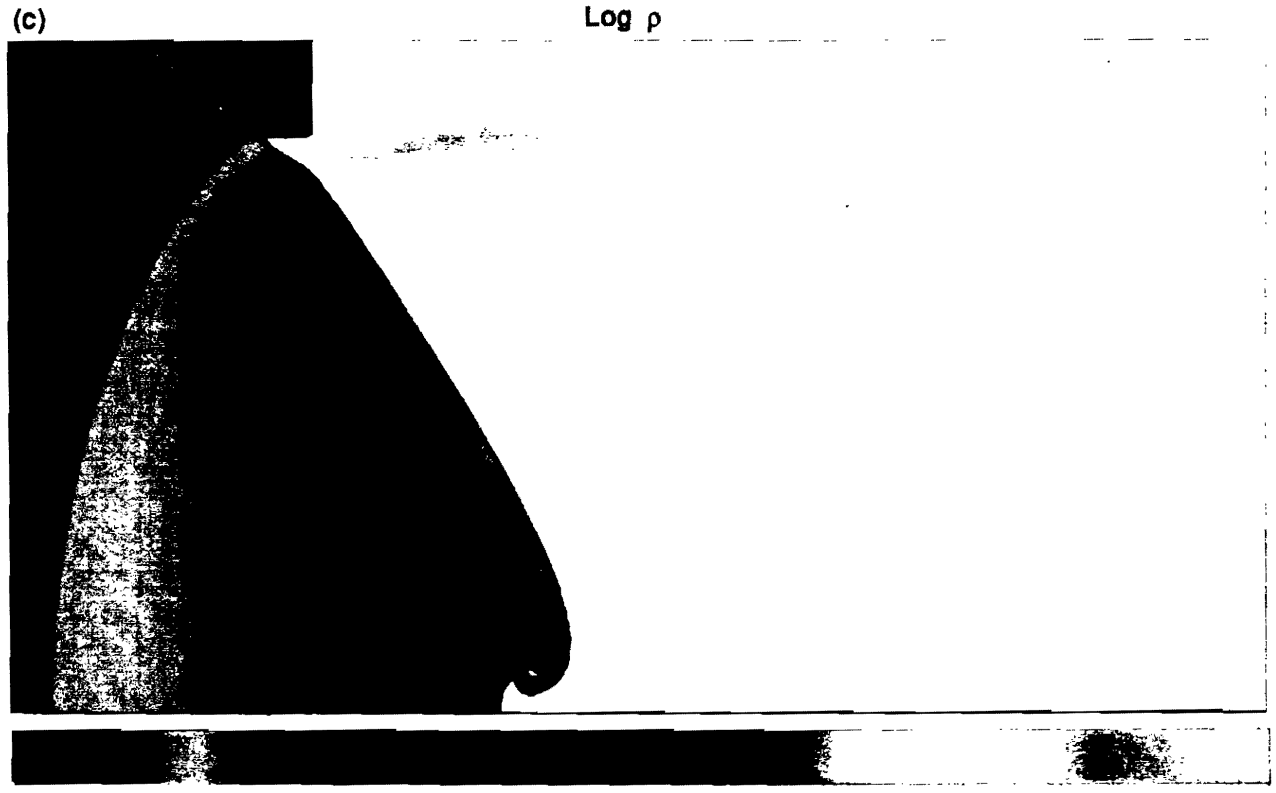

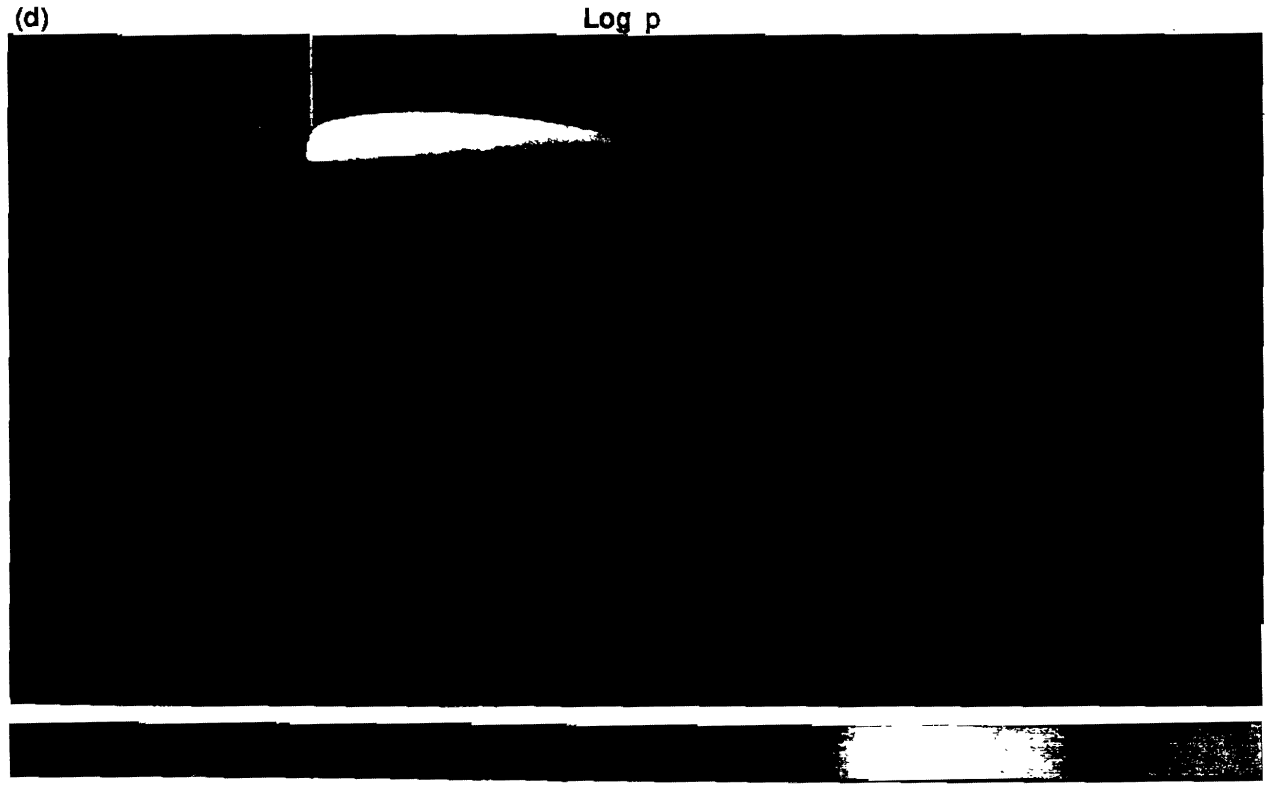

Fig. 13